THE CORONAL DIAGNOSTIC SPECTROMETER FOR THE SOLAR AND HELIOSPHERIC OBSERVATORY

R.A. HARRISON, E.C. SAWYER, M.K. CARTER, A.M. CRUISE, R.M. CUTLER, A. FLUDRA, R.W. HAYES, B.J. KENT, J. LANG, D.J. PARKER, J. PAYNE, C.D. PIKE, S.C. PESKETT and A.G. RICHARDS
Space Science Dept., Rutherford Appleton Laboratory, Chilton, Didcot Oxfordshire OX11 0QX, UK

J.L. CULHANE, K. NORMAN, A.A. BREEVELD, E.R. BREEVELD, K.F. AL JANABI, A.J. MCCALDEN, J.H. PARKINSON, D.G. SELF and P.D. THOMAS
Mullard Space Science Laboratory, University College London, Holmbury St Mary, Dorking, Surrey RH5 6NT, UK

A.I. POLAND, R.J. THOMAS and W.T. THOMPSON
NASA Goddard Space Flight Center, Code 682, Greenbelt, MD 20771, USA

O. KJELDSETH-MOE, P. BREKKE, J. KARUD and P. MALTBY
Institute of Theroetical Astrophysics, University of Oslo, PO Box 1029, Blindern, 0315 Oslo, Norway

B. ASCHENBACH and H. BRÄUNINGER
Max-Planck-Institut für Extraterrestrische Physik, D-85748 Garching, Germany

M. KÜHNE and J. HOLLANDT
Physikalisch-Technische Bundesanstalt, Inst. Berlin, Abbestrasse 2-12, D-1000 Berlin 10, Germany

O.H.W. SIEGMUND
Experimental Astrophysics Group, Space Sciences Laboratory, University of California, Berkeley, CA 94720, USA

M.C.E. HUBER
ESA, Space Science Dept., ESTEC, PO Box 299, 2200 AG Noordwijk, The Netherlands

A.H. GABRIEL
Inst. d'Astrophysique Spatiale, Université Paris XI, 91405 Orsay Cedex, France

H.E. MASON
Dept. Applied Mathematics and Theoretical Physics, University of Cambridge, Cambridge CB3 9EW, UK

and

B.J.I. BROMAGE
Dept. of Physics and Astronomy, University of Central Lancashire, Preston PR1 2HE, UK

Abstract. The Coronal Diagnostic Spectrometer is designed to probe the solar atmosphere through the detection of spectral emission lines in the extreme ultraviolet wavelength range 150 - 800 Å. By observing the intensities of selected lines and line profiles, we may derive temperature, density, flow and abundance information for the plasmas in the solar atmosphere. Spatial and temporal resolutions of down to a few arcseconds and seconds, respectively, allow such studies to be made within the fine-scale structure of the

Solar Physics **162**: 233–290, 1995.

solar corona. Furthermore, coverage of large wavelength bands provides the capability for simultaneously observing the properties of plasmas across the wide temperature ranges of the solar atmosphere.

Key words: Solar Atmosphere – Extreme UV Spectroscopy

1. Science Objectives

The two goals of the ESA/NASA Solar and Heliospheric Observatory (SOHO) which are concerned with the solar atmosphere are:

- How is the corona heated - why does it exist?
- How is the solar wind accelerated?

These goals underpin a desire to understand the nature of the solar atmosphere. They have wide-reaching applications since such questions have relevance to all stars and have relevance to an understanding of the solar-terrestrial system, since the Earth's environment is influenced by both solar radiation and ejecta. So, the goals of SOHO call for an extremely thorough study of the solar atmosphere, effectively calling for knowledge of the energy, momentum and mass balance at any location within a highly structured and dynamic system.

Critical to the pursuit of the goals of SOHO, then, is the determination of plasma characteristics (densities, temperatures, flow velocities, abundances etc...) with spatial, temporal and spectral resolutions and ranges appropriate to study the structure and evolution of the solar atmosphere.

The Coronal Diagnostic Spectrometer (CDS) is designed to determine such information through the study of emission line characteristics in the extreme ultraviolet (EUV) region of the electromagnetic spectrum. This region is particularly important for the detection of emission from the hottest plasmas of the (non-flare) solar atmosphere.

The performance requirements for CDS are determined by the characteristics of the solar atmosphere and by the nature of potential heating and acceleration mechanisms. They can be listed as:

- Wavelength coverage should include lines from ions formed in the temperature range 10^4 K to a few x 10^6 K. The region 150 - 800 Å is appropriate for this, the shorter wavelengths being essential for the inclusion of emission lines from the hottest plasmas.
- Spectral resolution should allow separation of the lines of prime interest. Given the crowded nature of the 150 - 220 Å region, inevitably there will be blends, but most lines of prime interest can be separated with a resolution of order $\delta\lambda$=0.3 Å, or $\lambda/\delta\lambda = 500$ at the shortest wavelengths.
- The field of view, without repointing, must be large enough to cover an active region or a large fraction of features such as prominences, coronal holes or quiet Sun. If the instrument cannot view the full Sun, re-pointing should allow studies of any region of the disc or low corona.

TABLE I
Density sensitive line ratios of prime interest

Ion	Wavelengths (Å)	Reference
Mg VI	314.55/400.68 & 314.68/400.68	Bhatia and Mason, 1980
Mg VII	319.03/278.40 & 280.74/278.40	Keenan *et al.*, 1986
Mg VII	319.03/367.67 & 319.03/429.93	Mason and Bhatia, 1978
Mg VII	280.74/429.93 & 320.50/429.93	Mason and Bhatia, 1978
Mg VIII	430.47/436.62	Dwivedi, 1988
Mg VIII	315.02/335.23, 315.02/430.47 & 436.62/313.74	Dwivedi and Raju, 1980
Si VIII	276.84/319.83 & 216.92/319.83	Bhatia and Mason, 1990
Si IX	349.87/341.95 & 345.13/341.95	Mason and Bhatia, 1978
Si IX	292.76/341.95 & 296.12/341.95	Mason and Bhatia, 1978
Si X	347.40/356.04	Dwivedi, 1988
S X	180.72/264.24 & 177.55/264.24	Bhatia and Mason, 1980
S XI	215.93/281.42, 190.37/281.42 & 217.64/281.42	Mason and Bhatia, 1978
S XII	288.41/299.50	Vernazza and Mason, 1978
Fe X	175.27/174.53	Jordan, 1965, 1966
Fe XI	180.41/181.14 & 184.41/181.14	Jordan, 1965, 1966
Fe XI	179.76/181.14 & 184.70/181.14	Dere *et al.*, 1979
Fe XII	186.87/193.51 & 196.64/193.51	Dere *et al.*, 1979
Fe XII	338.27/364.47	
Fe XIII	196.53/200.02	Dere *et al.*, 1979
Fe XIII	202.04/200.02 & 201.12/200.02	
Fe XIII	318.12/320.80	Dere *et al.*, 1979
Fe XIII	202.04/203.79 & 320.80/348.18	Mason and Young, 1994
Fe XIII	318.12/348.18 & 359.64/348.18	Mason and Young, 1994
Fe XIV	219.12/211.32 & 264.80/274.20	Jordan, 1965, 1966

- Spatial resolution must be down to a few arcseconds, appropriate for the smaller scale structures of the solar atmosphere.
- Time resolution should be as short as possible and certainly down to ~1 second.

1.1. Prime Emission Lines

The limitations of current technology mean that the full 150 - 800 Å wavelength range cannot be viewed simultaneously. Thus, to identify the prime wavelength regions the distribution of emission lines of particular interest has been studied. These studies have been restricted to emission lines which we may reasonably expect to detect and, in the case of the use of tempera-

TABLE II
Temperature sensitive line ratios of prime interest

Ion	Wavelengths (Å)	Reference
O III	702.98/599.59	Keenan *et al.*, 1989
O V	172.17/629.73	Malinovsky, 1975
O VI	173/1032* & 184/1032*	Heroux *et al.*, 1972
Ne V	359/572.20 & 365/572.20	Lang, 1988
Ne V	416.20/569.20 & 416.20/572.20	Keenan *et al.*, 1986
Mg IX	705.80/368.06 & 705.80/749	Doyle *et al.*, 1985
Si XI	604/580.90	Doyle *et al.*, 1985

* Viewed by the SUMER instrument on SOHO

ture and density senstive line ratios, involve intensity ratios which vary by a factor of at least 5 over the density/temperature ranges which one might expect to encounter. The lines of prime interest for CDS are listed in Tables I to IV. These include (i) ratios suitable for density and temperature analyses, (ii) element series particularly suited to temperature studies, and (iii) well separated, bright lines formed over wide temperature ranges, for dynamic analyses. An additional selection worthy of note is the availability of several high-temperature lines, e.g. Fe XXI at 270.52 Å and Fe XXIII at 263.76 Å.

2. Instrument Overview

The scientific requirements described above cannot be achieved with a single instrument, consequently CDS is a double spectrometer, having the advantages of the wide wavelength range of a grazing incidence device plus the stigmatic imaging performance of a normal incidence instrument (see earlier reports by Patchett *et al.*, 1989; Harrison and Sawyer, 1992, 1993).

The optical elements of CDS are shown in Figure 1. A grazing incidence Wolter-Schwartzchild type 2 telescope feeds simultaneously a normal incidence spectrometer (NIS) and a grazing incidence spectrometer (GIS) which share a common slit. As indicated by the light stop in Figure 1, between the telescope and the slit assembly, two portions of the telescope beam are selected, one for each spectrometer. In the NIS, after a single normal incidence reflection off two toroidal gratings, the in-coming beam is focused onto an intensified CCD detector, producing two spectrally dispersed stigmatic images. To build up larger images a plane mirror in front of the slit is scanned through a small angle in 2 arcsecond steps. The GIS comprises

TABLE III

Element series particularly suited to temperature analyses.

Ion	Wavelength (Å)	Log T (K)	Ion	Wavelength (Å)	Log T (K)
Ne I	735.90	4.4	Ne VI	401.14	5.6
Ne I	743.70	4.4	Ne VII	465.22	5.7
Ne III	489.50	4.9	Ne VIII	770.40	5.8
Ne V	482.10	5.5	Ne VIII	780.30	5.8
Ne VI	399.83	5.6			
Mg VI	399.20	5.6	Mg VIII	313.73	5.9
Mg VI	400.68	5.6	Mg VIII	317.01	5.9
Mg VII	277.04	5.8	Mg IX	705.80	6.0
Mg VII	278.40	5.8			
Si VII	272.60	5.8	Si IX	296.12	6.0
Si VII	275.37	5.8	Si IX	345.12	6.0
Si VIII	319.83	5.9	Si X	261.06	6.0
Si VIII	316.22	5.9	Si X	271.99	6.0
Fe VIII	168.18	5.6	Fe XII	195.12	6.2
Fe VIII	186.60	5.6	Fe XIII	203.79	6.2
Fe IX	171.07	6.0	Fe XIII	213.77	6.2
Fe IX	217.10	6.0	Fe XIV	211.32	6.3
Fe X	174.53	6.1	Fe XIV	220.08	6.3
Fe X	177.24	6.1	Fe XV	284.16	6.3
Fe XI	188.22	6.1	Fe XVI	335.40	6.4
Fe XI	192.81	6.1	Fe XVI	200.80	6.5
Fe XII	193.51	6.2			

a spherical grating set at grazing incidence, with four microchannel plate detectors placed around the Rowland circle. The resulting spectra are astigmatic. Thus, for GIS operation, pin hole slits are used and, to enable images to be built up the slits can be moved in one arcsecond increments in a plane perpendicular to the direction of dispersion, and the scan mirror moved in two arcsecond increments in the plane of dispersion.

The field of view of the telescope is 4 arcminutes. To cover the whole solar disc the instrument can be repointed through an angle of $\pm$ 0.75°. The instrument is supported on six legs; the front four are pivoted at each end and the rear two legs consist of linear actuators.

TABLE IV

Bright, well separated lines suitable for dynamic studies. The top portion of the Table corresponds to the Grazing Incidence ranges of CDS, and the bottom portion corresponds to the Normal Incidence ranges (see Table V).

Ion	Wavelength (Å)	Log T (K)	Ion	Wavelength	Log T (K)
O III	702.98	4.9	Fe X	174.53	6.1
N IV	765.14	5.0	Fe XI	188.22	6.1
Ne VI	401.14	5.6	Fe XII	195.12	6.2
Ne VII	465.22	5.7	Fe XIII	203.79	6.2
Ne VIII	770.40	5.8	Fe XIV	211.32	6.3
Fe IX	171.07	6.0	Fe XV	284.16	6.3
He I	584.33	4.3	Fe XII	364.47	6.2
O III	599.59	4.9	Fe XIII	320.80	6.2
O IV	554.52	5.3	Fe XIV	334.17	6.3
Ne VI	562.83	5.6	Fe XV	327.02	6.3
Mg VIII	313.73	5.9	Fe XVI	335.40	6.4
Mg IX	368.06	6.0			

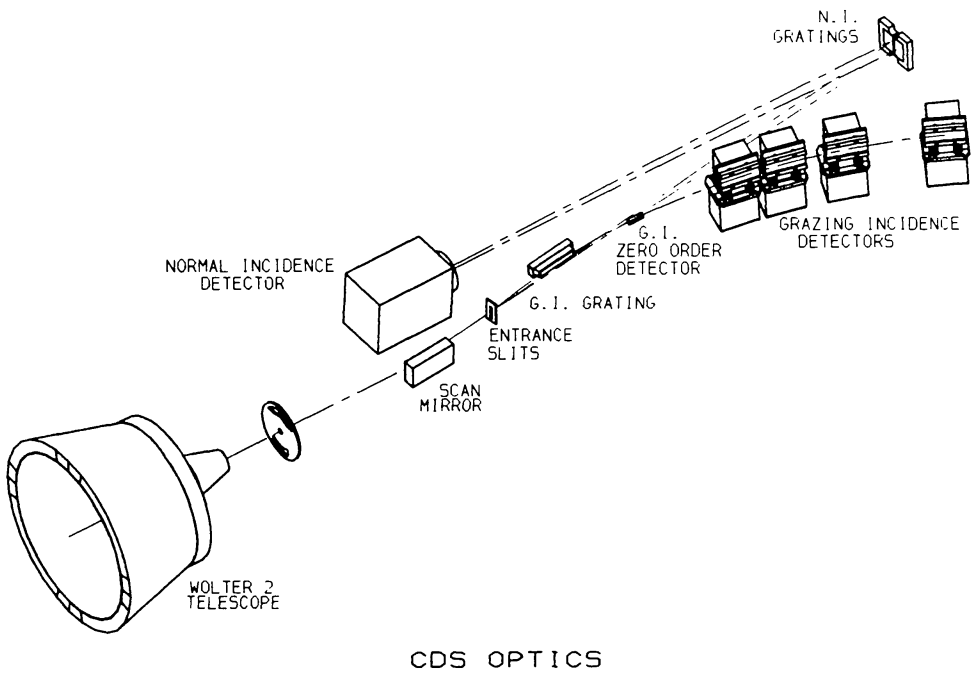

Fig. 1. The optical elements of CDS

All of the optical components with the exception of the telescope are housed in an enclosed optical bench, which is supported in a separate primary structure. The telescope, in its own container, is mounted at the front

of the primary structure. This arrangement allowed the optics to be sealed in a cavity that could be purged with clean gas at all times prior to launch. Doors over the two telescope apertures will be first opened well after the launch of SOHO, after the exterior of the instruments and spacecraft has completely outgassed.

Electronics units for the detector system and for mechanism control are mounted on a platform above the optics bench where they are thermally isolated from the rest of the structure and can radiate unwanted heat directly to space. Unwanted sunlight is intercepted at several points within the instrument and the heat conductively coupled to a space facing radiator. Two of the electronics boxes, the command and data handling system (CDHS) and the experiment power supply (EPS) are mounted on the spacecraft remotely from the instrument (see sections 5.2 and 7).

Pointing can be monitored through the use of a Sun sensor which is co-aligned with the telescope and mounted adjacent to the front Sun shield of the instrument.

Some general characteristics of CDS and its performance are summarised in Table V.

If one examines the performance of past EUV space borne instrumentation, it becomes clear that the CDS experiment represents the first thorough examination of the EUV Sun. EUV detectors have been directed at the Sun since OSO I in 1962, but if one demands (i) wavelength coverage extending to the 150 - 300 Å region, to include the emission from the hottest, coronal plasmas, (ii) *some* spatial resolution (i.e. not integrated Sun) and (iii) *some* spectral resolution (i.e. not integrated wavelength bands) only four experiments are found to satisfy these demands. These are the EUV OSO VII experiment (1972), the slitless spectrograph on Skylab (1973/4), the CHASE (Coronal Helium Abundance Experiment) on Spacelab II (1985), and the SERTS (Solar EUV Rocket Telescope and Spectrometer) rocket experiment.

Although the Skylab slitless spectrograph covered the wavelength range 171 - 630 Å, it could not be used to unambiguously separate spectral and spatial information. Also, it was photographic which provided a very restricting temporal resolution. The CHASE and SERTS instruments flew on the Shuttle and on a rocket series, respectively, and were thus of short duration. In addition, the SERTS flights to date used film, again, limiting the temporal capabilities. Finally, the spatial resolution of the OSO VII experiment was of order 20 arcseconds, some 7 times coarser than that of CDS.

It is clear that CDS is a unique device ideal for tackling the coronal goals of SOHO.

TABLE V
Principal Characteristics of CDS

General	Total Mass	100 kg
	Overall Length	1.7 m
	Average Power	58 W
	Telemetry Rate	11.3 kbit/s
The telescope	Outer f-number	9.38
	Eff. Focal Length	257.831 cm
	FWHM	< 2 arcsec
	Full Geometric Area	289.28 cm^2
	Plate Scale at Slit	12.5 μm/arcsec
Mechanism Details	Pointing	Anywhere on disc & low corona (max. 48 arcmin from Sun centre)
	Raster Step Sizes	E-W = 2.032 arcsec N-S = 1.016 arcsec
NIS	Telescope Aperture Used	34.3 cm^2 per grating
	Wavelength Ranges	308 - 381, 513 - 633 Å
	Prime Slits	2 x 240,4 x 240,90 x 240 arcsec
	Grating Ruling	2400 & 4000 lines/mm
	Slit-Grating Dist	736.5 mm
	Grating-Detector Dist	744.6 mm
GIS	Telescope Aperture Used	47 cm^2
	Wavelength Ranges	151 - 221, 256 - 338, 393 - 493, 656 - 785 Å
	Prime Slits	2 x 2, 4 x 4, 8 x 50 arcsec
	Grating Ruling	1000 lines/mm
	Rowland Circle Radius	750 mm

3. Optical Layout

Due to the high absorption cross section of all materials in the EUV, optical systems working in this wavelength range consist entirely of reflective surfaces. For wavelengths less than about 300 Å the normal incidence reflectivity of even the best materials (e.g. aluminium) becomes vanishingly small and thus glancing or grazing incidence reflections must be used. Indeed up to about 1000 Å, grazing incidence has advantages as does minimising the number of reflections.

3.1. Telescope

The CDS telescope is a Wolter-Schwarzschild type 2 design in which the incident beam first makes a grazing incidence reflection off the internal surface of a paraboloid and then another grazing incidence reflection from the external surface of a confocal hyperboloid. The range of glancing angles off the parabaloid, or primary mirror, is 12.6 - 17.3^o, and the range of angles off the hyperboloid, or secondary mirror, is 11.1 - 18.4^o. The two reflections fulfil the Abbé sine condition to minimise spherical aberration and coma, and the Schwarzchild deviation from true conics of revolution extends the field of view by improving the off-axis performance. The telescope, manufactured by Zeiss (Oberkochen, Germany), was constructed from zerodur, a highly stable glass ceramic with a very low coefficient of thermal expansion. The reflecting surfaces were polished to a surface finish of better than 10 Å rms and coated with gold. Deviations from the best fit profile are 10 +/- 2 nm (Schmidt *et al*, 1994).

The spatial resolution of such a telescope is effectively defined by the full width at half maximum intensity (FWHM) of the point spread function, that is the FWHM of the intensity distribution resulting from the observation of an infinitely distant point source. This was measured in the following way. A hollow cathode light source filled with helium (radiation principally at the wavelengths 304 and 584 Å) was placed behind a pinhole of size 5 μm, 125 m from the telescope. At the telescope focus, measurements were made with a 2-D intensified CCD detector, consisting of an open microchannel plate stack within, through the photoelectric effect, in-coming photons produce electron showers which, on arrival at a phosphor coating, are converted to visible light which is directed through a fibre optic to a CCD. Utilising a transputer driven centroiding algorithm the system is able to resolve down to the pore size of the microchannel plate (i.e. about 10 μm).

Figure 2 shows the profiles of the point spread function. Four traces are shown; for each of the NIS and GIS apertures of the telescope the point spread function is given in the direction of wavelength dispersion (Y) and the direction perpendicular to it (X). The FWHM values are 1.2 and 1.7 arcseconds, for the GIS aperture, in the Y and X directions, respectively. Similarly, for the NIS aperture, the values are 1.2 and 1.5 arcseconds. The half energy width in all cases is less than 5 arcseconds.

In addition, a measure of the large angle scatter of the point spread function gives an indication of the potential for intensity contamination from sources not in the line of sight. Figure 3 illustrates the large angle scatter performance of the telscope. The plot is produced from observations made at 68 Å and is normalised to unity to demonstrate the contribution at any point due to a source of intensity unity located at the core. The shape of the curve at distances from the core of less than 20 arcseconds is heavily

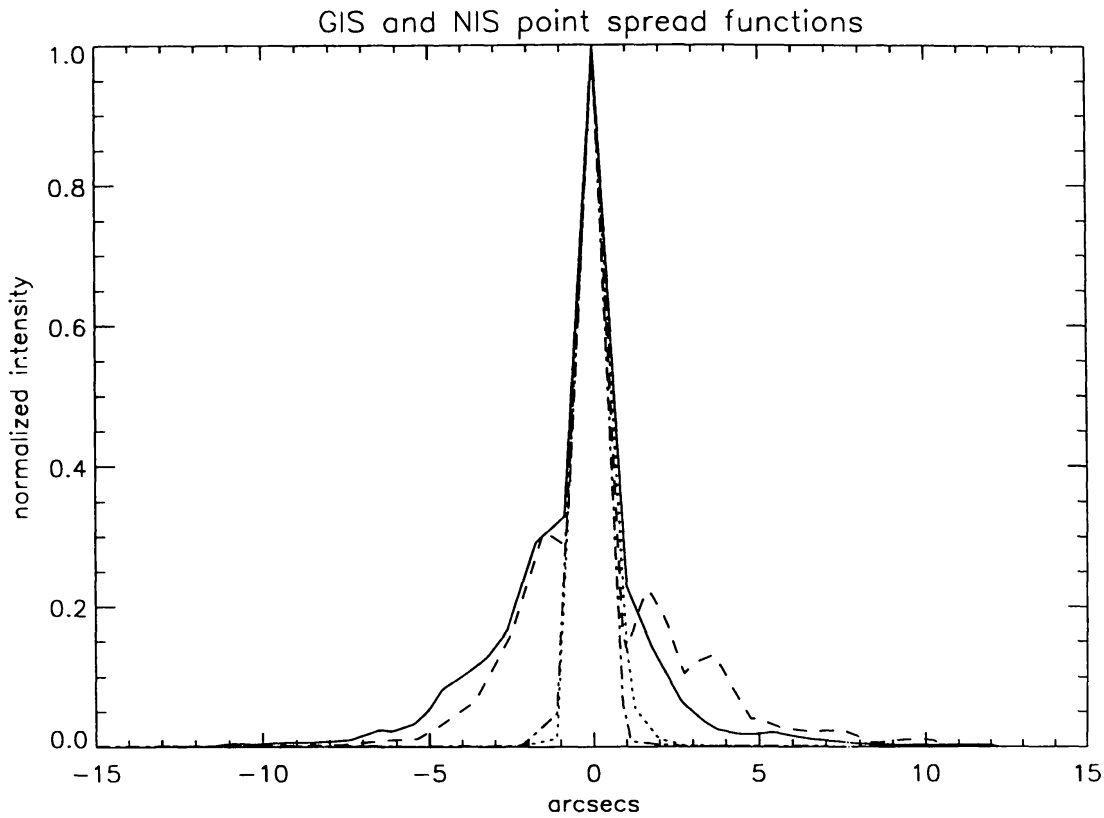

Fig. 2. The telescope point spread function: For the GIS and NIS apertures curves are given for the direction of wavelength dispersion (Y) (dash-dot and dotted curves, respectively) and the direction perpendicular to it (X) (dashed and solid, respectively).

influenced by the detector pixel size and should be ignored. However, values of order $10^{-4.3}$, $10^{-5.4}$, $10^{-6.2}$, $10^{-6.6}$, $10^{-7.8}$ and $10^{-8.5}$ are indicated for distances of 20, 50, 100, 150, 500 and 1000 arcseconds from the core (the last two values are not shown in Figure 3). Technical limitations resulted in no equivalent measurements at wavelengths more suited to the CDS range. However, in moving to longer wavelengths, the scatter is expected to be lower, by a factor of up to 5.

A Wolter 2 design is required because the small f number and flat focal plane provide a suitable match to the following GIS and NIS spectrometers. Instrument mass and size are a direct function of the f number and the sizes and resolutions of available detectors provide limitations on the divergence and reflection of instrument light paths.

The operational requirement of uninterrupted solar viewing whilst minimising instrument thermal gradients to ensure optimum optical performance places demanding constraints on the thermal design particularly in the high energy density regime of the converging beam incident on the telescope secondary (hyperboloid) surface. A system of conductive and radiative paths is used to remove excess heat from the telescope and maintain a secondary temperature of less than 40°C (see section 6).

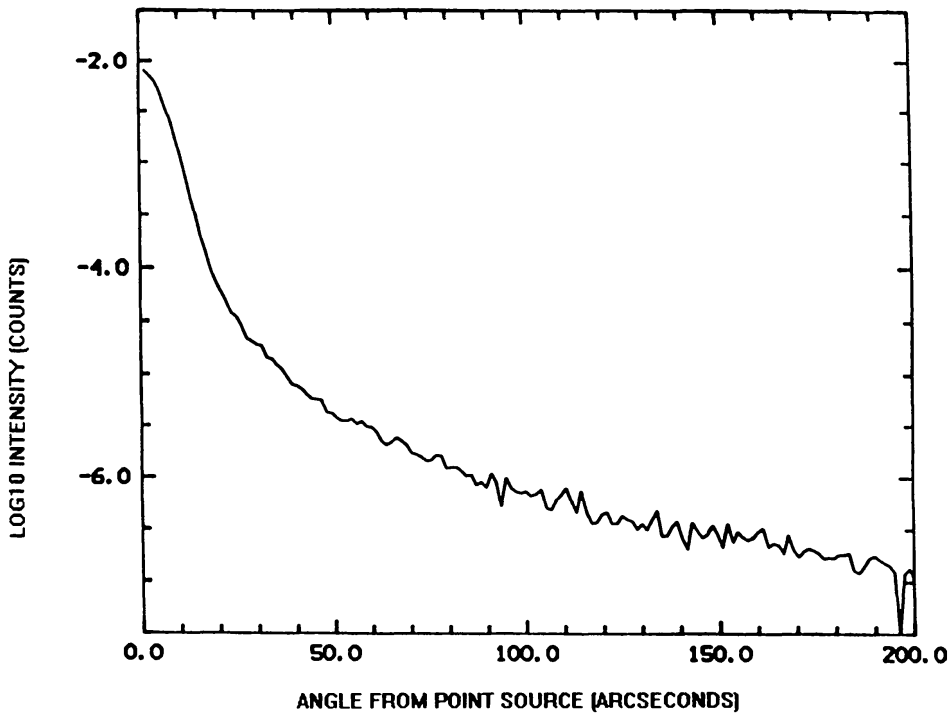

Fig. 3. The telescope large angle scatter at 68 Å for the region up to 200 arcseconds from the point spread function core.

Finally, only two portions of the Wolter telescope are used. Although the CDS telescope is a full-revolution system, apertures in a front panel define two light paths which ultimately feed the two spectrometers separately. Each aperture can be opened or shut by the use of dedicated doors.

3.2. Scan Mirror

The converging beam from the telescope is reflected at grazing incidence ($\sim 5^o$ angle) from a flat, premium grade zerodur, gold coated 160 x 35 x 20 mm scan mirror before forming an image at the spectrometers' entrance slit. Rotation through $\pm 0.3^o$ enables a region of interest in the solar image (± 2 arcminutes) to be scanned over the slit and thus we may construct in a piece by piece fashion spectrally selected maps or spectroheliograms. The surface quality of the scan mirror is comparable to that of the telescope ($\sim$ 10 Å rms roughness) and in its unconstrained form is flat to $\lambda/10$ waves (λ = 6328Å) with no local deviations greater than 2 arcseconds. 20% mass reducing pockets in the rear surface were included to reduce the pre-loads necessary for launch restraint. The scan mirror is kinematically mounted in an aluminium alloy holder and restrained at six points, pre-loaded to 17 kg in each axis to prevent movement during launch. This loading degraded the mirror form to $\lambda/2$ at room temperature but at operating temperature in orbit due to differential thermal expansion of the holder and zerodur

the pre-loads are greatly reduced. Positioning the scan mirror rotation axis through the reflecting surface is achieved by a pair of co-aligned flex pivots with counter balance used to remove off axis loads from the flex pivots during launch. The small angular rotation of $\pm 0.3^{\circ}$ is accomplished by a lever attached to the back of the mirror mount operated by a stepper motor operating through the wall of the spectrometer via a labyrinth seal. A single motor step is equivalent to a change in view direction of 2 arcseconds on the Sun.

3.3. Slits

The entrance slits of both spectrometers have a common location at the telescope focal plane. Six slits are available notionally designated as three for each spectrometer. They are listed in Table V. The GIS is astigmatic and thus the only method of achieving spatial resolution in the plane perpendicular to the dispersion direction is by means of a pinhole of the required spatial resolution. The grazing incidence slits are thus square apertures providing 2 x 2 and 4 x 4 arcsecond resolution. The stigmatic normal incidence system uses entrance slits which are long in the direction perpendicular to the dispersion plane, the spatial information contained in the length of the slit being retained by a 2 dimensional imaging detector. The normal incidence slits are thus slots of 2 x 240 and 4 x 240 arcsecond. The highest spectral resolution is obtained by using the narrowest slits, however for low intensity lines one can sacrifice resolution for improved throughput and use the wider slits. The two remaining slits have other functions. An additional factor of 100 in throughput is available for the GIS by using a 8 x 50 arcsecond slit, and a very large 90 x 240 arcsecond is available for the NIS to provide viewfinder images of the Sun simultaneously in several bright spectral lines.

The telescope plate scale of 12.5 μm/arcsecond gives the physical size of slits as 25 and 50 μm wide for 2 and 4 arcsecond. These are realised by electroforming 25 μm nickel foil attached to a 100 μm copper support and the whole attached by epoxy to an aluminium alloy support frame. A linear translation system enables any slit to be placed in position and also allows the slits to be scanned in 1 arcsecond steps. Thus the combination of slit scan and scan mirror motion allows spectrally selected images to be constructed in the GIS system. For the stigmatic NIS system only the mirror rotation is needed to construct images in several spectral lines simultaneously.

The slit mechanism is based on a stepper motor driving a precision carriage which carries the slit assembly. As in the scan mirror system the motor itself is mounted outside the spectrometer volume and drives the slit scan mechanism by a lead screw and recirculating ball nut. Contamination control requirements dictate the use of solid lubricants in this location and for reasons of particulate control we use a lead film system (see section 3.6).

3.4. Spectrometers

3.4.1. The grazing incidence spectrometer

The grazing incidence spectrometer (GIS) is a Rowland circle design based on a spherical grating of 1500 mm radius of curvature used at an angle of incidence of 84.75°, which disperses radiation onto four flat detectors placed around a Rowland circle of radius 750 mm. The circle is tangential to the grating at its centre and passes through the centre of the entrance slit. It defines the location at which specularly reflected radiation is brought to a horizontal focus - the zero order. The grating with a ruling density of 1000 lines per mm was produced using a replication process that starts with a mechanically ruled master and results in a replica on zerodur complete with a gold coating. The GIS grating was manufactured by Hyperfine, Colorado, USA. The rulings are blazed for highest 1st order efficiency at 350 Å. The four flat detectors are placed around the Rowland Circle such that their faces intercept the circle as chords, and occupy the wavelength intervals defined by their positions (Table V).

The characteristics of this configuration are given in Table VI for the shortest, middle and longest wavelength of each of the four GIS detector ranges. The first column lists the wavelength, λ. The location of a given wavelength on the Rowland circle is given by

$$n\lambda = d(sin\theta + sin\alpha) \quad (1)$$

where n is the order (equal to unity in the cases given), d is the grating spacing (see Table V), θ is the angle of incidence (84.75°) and α is the angle of reflection. The values for α are given in Table VI.

The instrumental contributions to the detected line width are due to the projection of the slit onto the flat detector, which is given by the slit width divided by the cosine of α (given in Table VI for the 25 μm slit), and the geometric defocus due to the mismatch of the flat detector and the Rowland circle curvature. These projected widths are listed in columns 3 and 4 of Table VI. The final width, calculated from these two contributions, is given in columns 5 and 6, in units of μm and pixels, respectively.

The spectral resolving power, $\lambda/\delta\lambda$, is derived by differentiating equation (1). Thus

$$\frac{\lambda}{\delta\lambda} = \frac{2\lambda R}{d\epsilon cos\alpha}. \quad (2)$$

R is the radius of the Rowland circle (see Table V) and ϵ is the scale of the resolving element, in this case the line width. The resulting spectral resolution is given in column 8 and the wavelength dispersion in column 9.

The GIS system also includes a zero order detector consisting of a very well baffled photo transistor behind a 50 μm wide slit. This intercepts the specularly reflected (i.e. undispersed) radiation and serves to support in-flight calibration of the CDS solar pointing system by enabling solar limb

TABLE VI

The Grazing Incidence Spectrometer resolution (for explanation, see text)

λ (Å)	α (Degrees)	Slit (μm)	Defocus (μm)	Width (μm)	Width (Pixels)	$\lambda/\delta\lambda$	$\delta\lambda$ (Å)	Disp. (Å/mm)
151	78.7	128	102	163	6.5	709	0.21	1.29
186	77.7	117	94	150	6.0	873	0.21	1.40
221	76.8	109	87	139	5.6	1044	0.21	1.51
256	76.0	103	83	132	5.3	1201	0.21	1.59
297	75.0	97	77	124	5.0	1392	0.21	1.69
338	74.2	92	73	117	4.7	1588	0.21	1.79
393	73.0	86	69	110	4.4	1837	0.21	1.91
443	72.1	81	65	104	4.2	2077	0.21	2.02
493	71.2	77	62	99	4.0	2314	0.21	2.12
656	68.5	68	54	87	3.5	3082	0.21	2.41
721	67.5	65	52	83	3.3	3401	0.21	2.53
785	66.5	63	50	80	3.2	3697	0.21	2.63

crossing detection. The zero order detector is sensitive to the wavelength range 5000-9500 Å, with greatest sensitivity at 8000 Å.

3.4.2. The grazing incidence detectors

Because of the astigmatic nature of the GIS the detectors are required to have a 1 dimensional (1-D) capability only. The basic requirements are as follows:

- All detectors identical so that they are fully interchangeable;
- position resolution of 47μm over a sensitive area of 50 x 16 mm;
- quantum efficiency greater than 10% ;
- maximum event rate of 100,000 ct/s random; and
- pixel width of 25 μm.

Figure 4 shows the layout of the GIS detector. The sensitive area of the detector is an open Z-stack of three microchannel plates (MCPs) which act as a photomuliplier. Each EUV photon produces a cloud of $\sim 4 \times 10^7$ electrons. Behind the MCP stack, a Spiral Anode (SPAN) detector receives the electron cloud and gives its position to 11-bit resolution in one dimension, i.e. along the direction of wavelength dispersion (Breeveld *et al.*, 1992).

The detectors are placed such that the longer axis is aligned in the direction of dispersion of the GIS spectrum. To prevent shadowing of the dispersed radiation, no clamping of the MCPs is allowed along the short edges

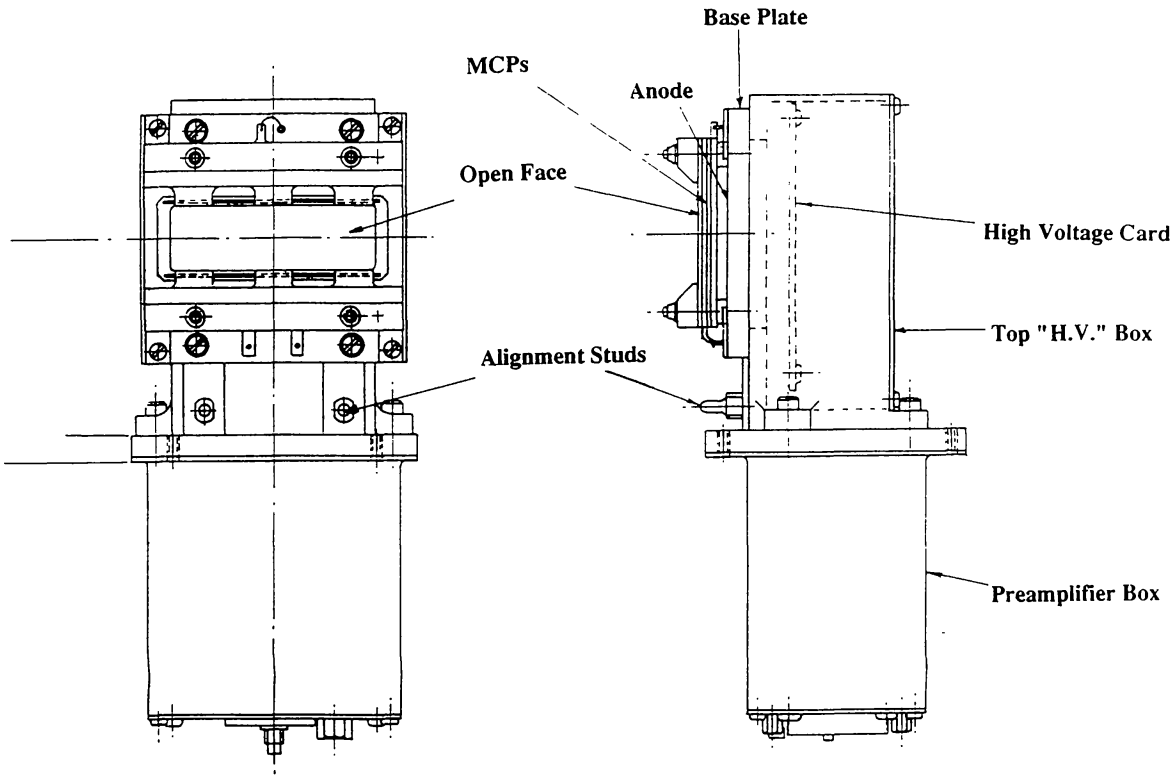

Fig. 4. Detector head, high voltage box and preamp box

and no repeller grid can be used to enhance the quantum efficiency. The MCPs are therefore used in an 'open face' configuration and are 50 mm x 25 mm with 4.2 mm used for clamping along the long edges.

To optimise the angle of incidence of the radiation on the MCP, the pores (each 12.5 μm diameter on a 15 μm web) are angled 13° To achieve the high count rate whilst minimising power and mass, a SPAN anode is used, because it only requires two 8-bit Analogue-to-Digital Converters (ADCs) to give the required 11-bit positional information. SPAN anodes are divided into horizontal pitches; each one identical and containing elements of 3 electrodes whose areas have the form of damped sine waves. Figure 5 shows the electrode confinguration.

The anode is made by coating a 63 x 30 x 3 mm piece of fused silica with a very thin layer of chrome followed by a 2 - 3 μm layer of aluminium. Metal is removed using an infrared Nd-Yag laser to form the insulating gaps between the electrodes. The laser position is precise to better than 1 μm. The electrode parameters (pitch height, minimum width etc.) have to be carefully matched to the spatial extent of the charge cloud emanating from the MCP's. After study, the chosen parameters are a pitch of 390 μm and

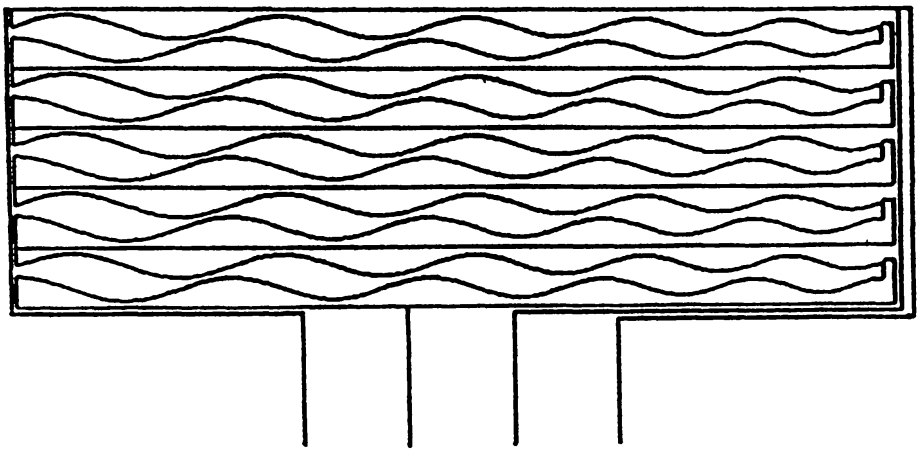

Fig. 5. A schematic of the 1-D SPAN anode electrode configuration

a minimum electrode width of 40 μm. The MCP-anode gap is 3mm with $\sim$ 350 V accelerating potential.

The front face of the MCP stack is kept near ground potential to avoid a high background due to ambient electrons or ions. Therefore the anode is held at high positive voltage. The voltage between the front of the MCPs and the anode is variable up to 5 kV with up to 4.3 kV across the MCPs. A resistive bias chain in parallel with the MCPs maintains plate potentials, improving stability with respect to temperature variation and aging of the plate. The front face is given a small potential, (-12 V) to repel low energy photoelectrons, and +12 V can be applied for use when 'flat fielding' using one of two electron-emitting filaments mounted within the optical bench.

Two copper strips are set into the base plate behind the anode. They can be stimulated with pulses of up to 5 V, at a rate of 104 c/s. The capacitive coupling with the anode, through the fused silica, provides signals from two stable positions and can be used to test the entire electronics chain at any time.

At any position along the anode the ratio of the charge collected on one electrode (X/(X+Y+Z)) to that collected by another electrode (Y/(X+Y+Z)) is unique. Two electrodes are therefore used for measurement, the third for normalising. After the charge from the MCPs lands on the electrodes it is collected by charge sensitive preamplifiers, shaped, amplified, peak-detected and summed. The sum signal drives the reference input of two low power 8 bit quasi-flash ADCs used to determine the required ratio. The sum is also digitised and used directly for building up a pulse height distribution (PHD). Finally the ratios are passed into a look-up table which gives the one dimensional location of the event. The look-up table will be monitored and calculated regularly on board by fitting parameters to raw data. The calcu-

lation of each position in real time would take too long given the expected count rates.

Data from the four detectors are formed one event at a time into a common 13 bit serial stream, giving 11 bits per detector. This gives 2048 "pixels" of size 25μm. However, the actual resolution performance of the detector is best described by the modulation transfer function (MTF) which describes the detector's ability to separate the peaks and troughs from a given square-wave distribution. The measured MTF distribution is given in Figure 6 for the GIS detectors. This measurement was performed using the electron-emitting filaments, rather than EUV light, though the results should be similar. In effect, once the square-wave pattern has been diluted by an appropriate distribution function relating to the performance of the detector, the MTF measures the ratio of the peak minus trough intensity divided by the sum of the peak and trough intensity. Thus, high values indicate good resolution and low values, poor resolution. The MTF is usually plotted against the *line pairs/mm* of the square wave distribution. For comparison, the abscissa values of 20, 15 and 10 line pairs per mm, correspond to peak to peak separations of 25, 33 and 50 μm. The limiting resolution is determined by the Nyquist frequency of the detector "pixels". In other words, if the square-wave wavelength is of order two pixels, we cannot detect a trough between the peaks. This limit, for 25μm pixels, is 20 line pairs per mm. In a low-noise system such as this, it is quite feasible to recover data with MTF values of down to 10%. This level is reached at approximately 18 line pairs per mm, i.e. a resolving element scale of 28 μm or 2.24 arcseconds.

The data stream is clocked at 1.25MHz and gives a maximum continuous count rate of 8.9 x 10^4 events per second. A bi-directional serial interface working at 62.5 kbits s^{-1} provides a 16 bit wide channel for commands to the detector system, and status and health monitoring back to the instrument controller. The entire detector system (four detector heads, four programmable high voltage units, and the support processing) consumes a total of 13W from the +5V, $\pm$12V, and +27V power lines.

For normal operation the science path uses non-programmable circuitry in order to ensure fast operation. The processor is then free to carry out the control and housekeeping functions.

An event trigger channel provides the timing for pulse-pair coincidence rejection. The measured rejection interval being 50 ns. Real events are discriminated from noise by a lower-level discriminator whose charge thresholds are programmable in eight steps ranging from 1.4 x 10^7 to 3.5 x 10^7 electrons. An upper-level discriminator, with charge threshold fixed at 8 x 10^7 electrons, inhibits AD conversions of over-energetic events and increments a counter in the science data processor hardware. The raw event rate and the output rate are both counted.

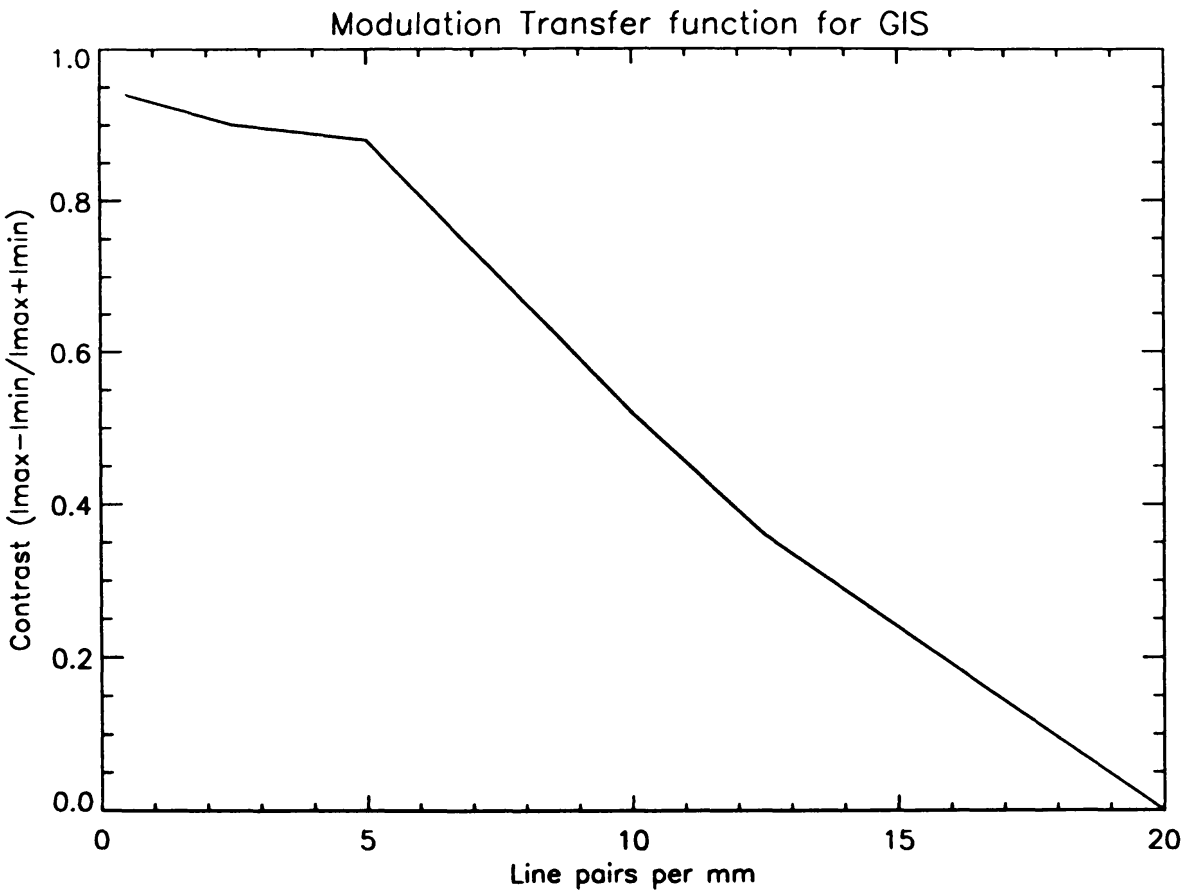

Fig. 6. The square wave Modulation Transfer function for the GIS detector, made using square hole masks with wavelengths of 25, 40, 50, 100, 200, 500 and 1000 μm

The analogue processing has two inherent dead-times. The first is the pre-event dead time T_w which accommodates settling of pulse shaping amplifiers and caters for the rejection of pulse pile-up. The second is the post-event dead time T_p. This prevents pile-up while the event pulse analogue to digital conversion is in progress. An event occurring in less than T_p after the current event invalidates the current event. A subsequent event occurring during either dead time will extend (retrigger) it a further time period T_w or T_p.

In the GIS detector system the values of T_w and T_p are 1.5 μs and 0.6 μs respectively, giving an additive extending dead time of 2.1 μs. From the classical formula for 'extending' dead time the theoretical maximum output rate R_o in terms of input rate R_i is

$$R_o = R_i exp(-R_i(T_w + T_p)).$$

The value of R_o has a maximum when $R_i = 1/(T_w + T_p)$ i.e. $R_i = 4.75\text{x}10^5$ cts/s. At maximum throughput $R_o/R_i = 1/e$. The detector high voltage supply and electronics are designed to accept short bursts of pulses at input rates of greater than 4.75 x 10^5 c/s but pulse pile-up in the charge amplifier

will occur if higher rates are sustained. The high voltage supply is designed such that charge depletion within the microchannel plates is insignificant.

3.4.3. The normal incidence spectrometer

The normal incidence spectrometer (NIS) is essentially a Rowland circle design with the exit beam direction along the Rowland circle diameter and thus has similarities to a Sirks configuration. Radiation from the entrance slit is incident at a mean angle of 7.9° onto a pair of toroidal gratings and is dispersed by them onto a 2 dimensional imaging detector such that the detector views along the normal to the center of the grating pair. The use of toroidal gratings at near normal incidence over a small wavelength range produces images (of the radiation at the entrance slit) that are essentially free of astigmatism and thus provides good spatial resolution, as well as high spectral resolution. The decreasing reflection efficiency at normal incidence with decreasing EUV wavelength limits the range of the NIS to wavelengths above 300 Å.

The two NIS gratings, mounted side by side as effectively two parts of the same surface, have different ruling densities such that for approximately the same incident and exit angular range they disperse two different wavelength bands, namely 310 - 380 Å and 520 - 630 Å. By imposing a small out-of-plane tilt in each of the diffraction gratings the two spectral bands are simultaneously displayed on the front surface of the same imaging detector, but displaced in the direction perpendicular to dispersion so that the two spectra appear stacked one above the other.

As for the GIS gratings, the NIS pair were made by Hyperfine, using a multistep process of deformation of replicas from mechanical rulings on a spherical master. The final gratings were fourth generation epoxy replicas with a gold coating. The curvatures of the two gratings are identical, i.e. radius of curvature in dispersion plane (major radius) 743.6 mm and in the perpendicular direction (minor radius) 736.4 mm. The ruling densities are 2400 and 4000 lines per mm for the long and short wavelength bands respectively, both blazed at 4°. These gratings were studied in some detail in order to measure their performance in the EUV, using radiation from the SURFII electron storage ring at the NIST (Boucarut *et al.*, 1993).

Since the NIS operates in near normal incidence, with angles of reflection between 7° and 9°, the projected slit width on the detector is represented by the actual slit width divided by the cosine of the angle of reflection, which is almost unity. Thus, the projected NIS slit width is of order 25.2 μm for the narrowest slit which, given the NIS detector pixel size of 21 μm represents 1.2 pixels. A summary of the resolving powers for the bottom, middle and top wavelengths of each range are given in Table VII. The values are derived using equations 1 and 2 and data from Table V.

TABLE VII

The Normal Incidence Spectrometer resolution (for explanation, see text)

λ (Å)	α (Degrees)	Width (μm)	$\lambda/\delta\lambda$	$\delta\lambda$ (Å)	Disp. (Å/mm)
308	7.08	25.2	3635	0.08	3.17
345	7.92	25.2	4080	0.08	3.17
381	8.75	25.3	4500	0.08	3.17
513	7.08	25.2	3635	0.14	5.56
573	7.92	25.2	4080	0.14	5.56
633	8.75	25.3	4500	0.14	5.56

3.4.4. The normal incidence detector

The detector for the NIS, known as the Viewfinder Detector Subsystem (VDS), is an intensified CCD camera built by Advanced Technology and Research Corporation in Laurel, Maryland (Thompson *et al.*, 1992). Compromises between scientific desire and engineering capabilities for space flight hardware have resulted in a detector with the following basic capabilities:

- Field of view represented by $\sim$ 1024 (spectral) x 512 (spatial) pixels;
- resolution $\sim$ 23 line pairs per mm, i.e. 21 μm pixels;
- detector quantum efficiency (DQE) in the 300 - 650 Å range $\sim$ 20% ;
- noise levels allowing for the minimum detectable flux of $<$ 0.01 photons/pixel/s (dark current of less than 0.01 photons/pixel/s);
- a maximum solar flux level of $> 10^5$ photons/pixel/s; and
- the ability to get time resolution down to 1 s or less.

The basic design of the detector head is shown in Figure 7. It consists of three basic modular components, the image intensifier (consisting of a microchannel plate (MCP) and phosphor converter to visible light), a lens and the CCD.

At the front of the detector, a windowless microchannel-plate intensifier tube detects and converts the EUV radiation to electrons, which are intensified in the MCP wafer, and then converted to visible light via a standard P-20 phosphor coated on the fibre-optic output window. The microchannel plate selected for this application was a Philips device with 12 μm channels on 15 μm spacing. No photocathode material is used; instead the detector relies on the photoelectric effect directly from the MCP (Siegmund *et al.* 1985). The MCP is operated in the range from approximately 600 V to 950

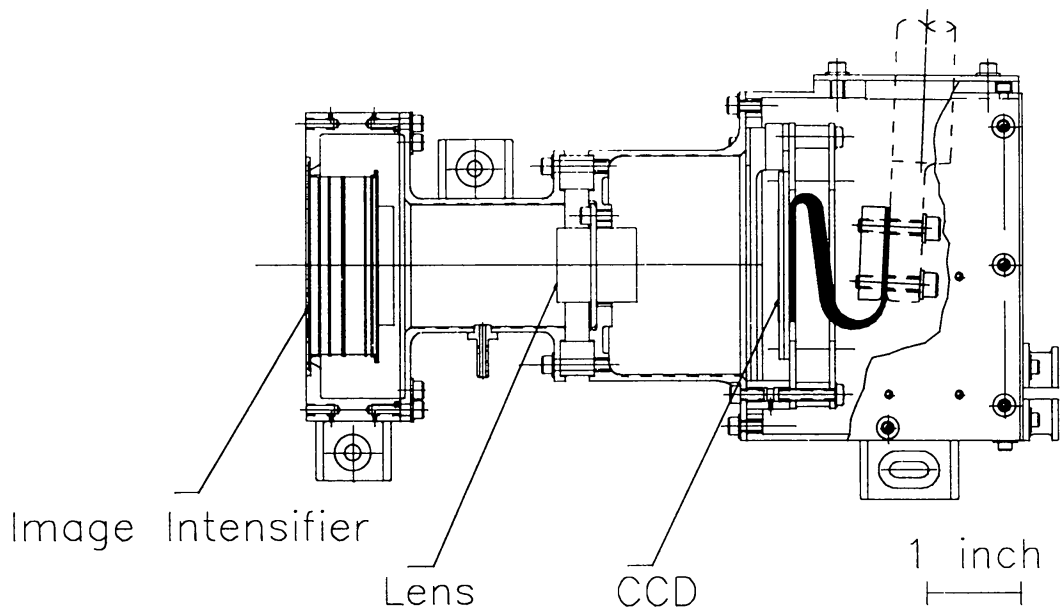

Fig. 7. VDS detector head assembly design, showing the MCP intensifier, the lens assembly, the CCD, and the cold strap and finger

V depending on the gain needed for the particular observation. It also acts as the system shutter when the voltage is dropped to $\sim$ 300 V.

A custom lens system built by Continental Optical Corporation focuses the intensified visible light onto a Tektronix 1024 x 1024 CCD with 21 μm square pixels. A heat-conductive strap attached to the back of the CCD chip is designed to transport the heat from the CCD to a radiative cooler attached to the side of the CDS instrument. The design operating temperature of the CCD is - 70° C to reduce dark current and the effects of radiation damage (Janesick et al. 1989). This has no influence on the detector sensitivity which is driven by the efficiency of the MCP.

The detector is run in integrating mode, that is, well within the linear regime (of MCP voltage vs MCP amplification) with an amplification orders of magnitude below that used for photon-counting. Hence, the detector can deal with the high count rates expected.

The CCD is operated in multi-pinned phase mode for reduced thermal background noise, and in 4-quadrant mode for shortest possible readout times. It can be operated in a number of different configurations, including readout through 1, 2 or 4 ports, and pixel binning. Selected windows can also be read out to improve the time resolution. CCD bias voltages are software programmable. This flexibility in camera operation is possible through the use of a microprocessor for all camera timing and provides some redundancy (multiple readout channels) in recovering from component failures.

The absolute quantum efficiency of the MCP image intensifier and converter was measured and is given in Figure 8. The quantum efficiency in the

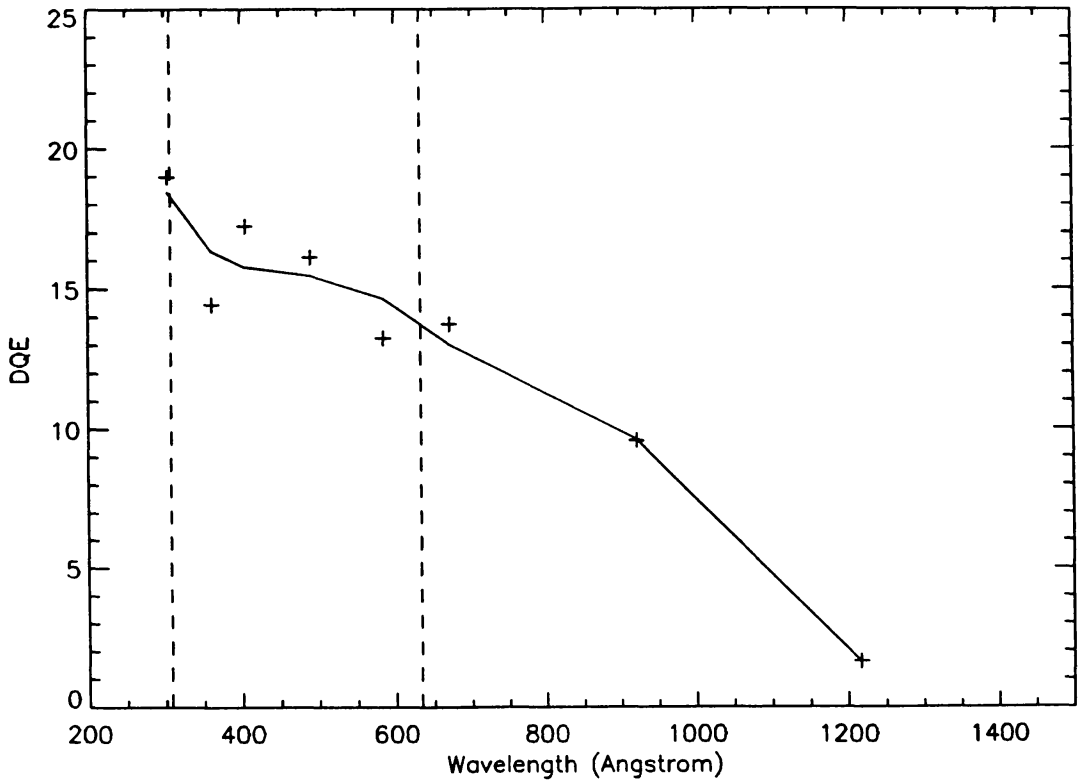

Fig. 8. The detector quantum efficiency as a function of wavelength. The crosses indicate measurements made at 304, 361, 405, 490, 584, 671, 920 and 1216 ÅThe dashed lines show the limits of the limits of the NIS wavelength range.

wavelength region of interest, 300 - 650 Å, is close to 20%. The low quantum efficiency at the H I Lyman-α line at 1216 Å is desirable to reduce the effect of any scattered radiation inside the spectrometer. The error on these values is of order 10-15% , mainly due to absolute errors in the reference source.

The ultimate detector resolution is limited by a combination of the MCP intensifier tube and the CCD. As with the GIS detector, we show the measured MTF of the detector, in Figure 9. The MTF is plotted for the VDS detector for observations made using a Krypton lamp with dominant emission at 1236 Å. For comparison, the abscissa values of 20, 15 and 10 line pairs per mm, correspond to peak to peak separations of 25, 33 and 50 μm.

Curves for both vertical and horizontal resolution are shown—they are very similar within the limits of the test. The limiting resolution, determined by the Nyquist frequency of the CCD pixel pattern, is $\sim$ 23 line pairs per mm (22 μm pixels). The slope of the MTF between approximately 5 and 20 line pairs per mm is due to the microchannel plate MTF.

The VDS detector is a very low noise system and thus can resolve even where the MTF is low. It is quite feasible to recover data with MTF values of order 10% , and even less. Thus, the CDS target of achieving a pixel

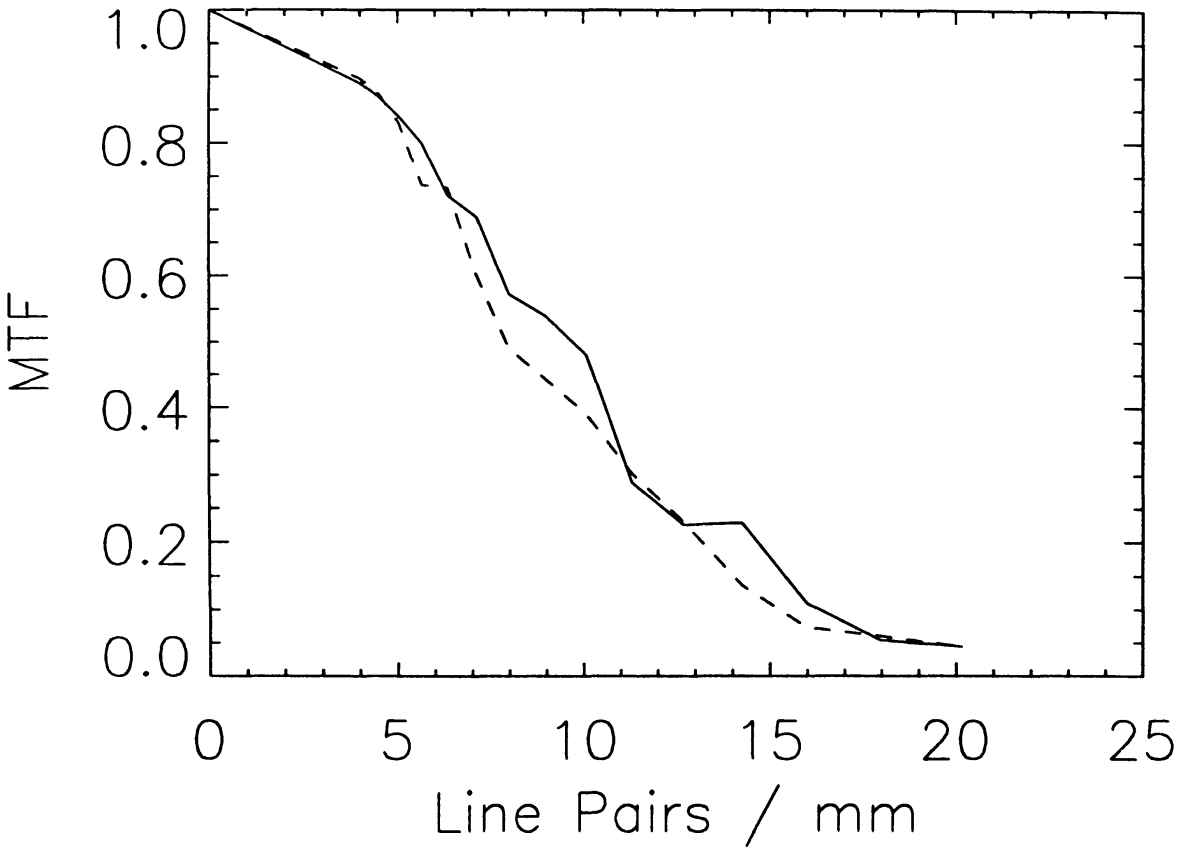

Fig. 9. Square-wave modulation transfer function based on an image of an Air Force resolution target. The solid line represents the resolution in the horizontal direction, and the dashed line is for the vertical direction.

element of order 3 arcseconds, which translates to 37.5 μm, is equivalent to a measurement at 13 line pairs per mm, where the MTF is still as high as 20% . The MTF curves suggest that we are doing much better than this, with the 10% level at about 16 line pairs per mm, i.e. grid spacings of 31 μm or 2.5 arcseconds.

Throughput tests of the VDS flight detector were done at programmable voltages of approximately 600 V, 678 V, 756 V, 834 V, 912 V, and 990 V. We define the throughput of the detector as the number of Analogue-to-Digital Conversion (ADC) counts for each photon that interacts with the MCP. In essence, this is a measure of the amplification of the detector. The total number of ADC units is proportional to the quantum efficiency times the throughput. The throughput for the VDS detector for various voltages is shown in Table VIII.

The VDS detector uses electronic shuttering. The voltage on the MCP is switched between the desired voltage during integration and a rest voltage between integrations. The rest voltage of the VDS flight detector was measured as 331V. Although no measurements of the VDS sensitivity were made with the MCP shuttered off, one can extrapolate the figures in Table

TABLE VIII

Detector throughput as a function of MCP voltage

Voltage	Throughput (ADC/photon-event)
600	0.256
678	0.820
756	2.43
834	6.69
912	15.1
990	35.0

VIII and estimate that the "off" sensitivity of the VDS detector is less than 0.005 ADC/photon-event.

The linearity of the VDS detector measured "intensity" with incident photon flux, was measured by placing a series of calibrated apertures in the collimated beam between the source and the detector. The resulting images were compared to a reference image taken with the smallest aperture and the lowest operating voltage, to ensure that this reference image was taken under linear conditions. It was found that if one multiplied the number of photon-events/pixel/s by the throughput given in Table VIII, thus generating the predicted number of ADC/pixel/s if the detector were linear, then the curves for all the MCP voltages merge into a single curve. The data demonstrate a linear relationship between ADC/pixel/s and the product of the throughput and the photon events/pixel/s, up to $\sim 5 \times 10^3$ ADC/pixel/s. After this point the linearity falls off. We were able successfully to fit the non-linearity characteristics of the detector using the function

$$F = \frac{R + (R/R_0)^P}{T}$$

where F is the number of photon-events/pixel/s, R is the system response in ADC/pixel/s, and T is the throughput from Table VIII. The fitted parameters are $R_0 = 904.0$ and $P = 4.1945$.

The photon counting Poisson statistics inherent in the incident photons themselves and the shot noise produced within the image intensifier dominate the noise in the VDS detector. The shot noise represents the amount of variability in the amplification process, which is a strong function of the voltage across the MCP. For a given MCP voltage, both the Poisson statistics and the shot noise should be proportional to the square root of the number of photons collected.

The full well capacity of the Tektronix CCDs used in the VDS detector were typically about 150,000 e^-. However, the actual upper limit on the data returned from the flight detector was imposed by the 12 bit AD converter, which had an upper limit somewhat below the CCD full well capacity. Combining this information with the data on noise, one obtains that the dynamic range of the VDS flight detector in a single exposure is $\sim$ 2000:1. A greater dynamic range can be achieved by taking multiple images with different exposure times.

3.5. Straylight Control

There are two aspects to straylight control in the CDS instrument. One is concerned with spatial contamination, where EUV light from the Sun's disc and corona is scatterred into the area of the Sun's image which is being viewed. The other is spectral contamination, where EUV light from wavelengths other than those selected is scattered and superimposed onto areas of the detectors being viewed.

Spatial stray light contamination can to a certain extent be kept low by a suitable design of the structure surrounding the light path through the optics, but it can ultimately be minimised only by procurement and maintainance of very clean, very high quality low-scatter telescope and scan-mirror optical surfaces. The CDS cleanliness control activities described above (see section 3.6) are conducive to this goal.

Amongst the design contributions which help to minimise this spatial contamination are careful design and placement of the aperture stop, the scan-mirror holder, grating holder surfaces and grating masks, the latter enabling rejection of scattered radiation components which may enter the entrance slit area but are travelling in directions somewhat different from those rays which travel the desired specular reflection paths through the telescope to the slit.

It was particularly important to ensure that the majority of solar radiation which reaches the spectrograph entrance slit plane and which is outside the field of view defined by the entrance slit area is prevented from entering the spectrometers. This unwanted component may be 10,000 to 100,000 times brighter than the signal entering the smaller slits.

Ideally, the spectrometer would be sealed off completely from the telescope, with only the slit between them. This was not possible because of the complex movable slit plate and because of the need to vent the air from both volumes, during launch.

Spectral contamination is probably the biggest problem encountered in the CDS instrument. The major problem is the H I Lα 1216Å radiation, which will enter both spectrographs with a much higher flux level than any spectral line or group of lines covered by CDS. For example, it is 20 times brighter than the brightest emission line in the CDS wavelength range, the

He II Lα 304 Å line. Moreover, the sum of the coronal emission lines between 9-610Å omitting the He II line, is still a factor of 8 times weaker than the 1216Å flux. The vast majority of the radiation reaching the gratings and detectors will be UV, visible and infrared, and fortunately, the CDS detectors are blind to this radiation. Stray radiation must not be allowed to encounter low-work-function photoelectron-emitting surfaces because the detectors will respond to electrons.

The only good defences against a 1216Å-induced detector background level are (a) very clean, very high quality low scatter grating surfaces (which the detectors view directly) and (b) efficient dumping of the unwanted 1216Å orders diffracted from the grating. The baffle design of both spectrometers incorporates the straylight control philosophy that no detector has a view of a surface directly illuminated by zero- or other order 1216Å radiation. Those surfaces which receive the 1216Å radiation have a proven very low scattering efficiency at this and other EUV wavelengths; aluminium alloy with Alochrome 1200 treatment was selected. Internal baffles have been added to both spectrometers to control this large unwanted energy component. Attention was also paid in the design process to those orders diffracted from the NIS grating which could re-enter the GIS spectrometer volume.

Another problem forseen for the GIS was the possibility that radiation from its grating which reaches one detector could be scattered/reflected towards other detectors. The probability for this occuring is finite due to the relatively high angles of incidence. Inter-detector baffles were therefore added to the GIS spectrometer design to prevent one detector from directly viewing the surface of any other detector. One baffle specifically controls any unwanted 2nd order He II 304Å radiation.

The control of scattered light in the NIS is made easier by the location of the single NI detector at the end of a long tube which could be fitted with baffles at intermediate locations. These baffles permitted a much better level of separation between those surfaces the NI detector could directly view and those surfaces which are directly illuminated by unwanted radiation. Conversely, the more open design of the GIS, with four wide-area detectors in close proximity, prevented the achievement of quite as high a level of shielding against unwanted radiation.

The general rules followed in designing CDS in order to minimise straylight contamination are summarised as follows:

- Minimise the area of illuminated non-optical structure.
- Ensure that detectors cannot view illuminated non-optical structure (either directly or via specular reflection from one or more optical surfaces or via a reflection at high angles of incidence from non-optical surfaces).

- If, during the design process, it appeared that an illuminated non-optical surface could be directly seen by the grating or a detector, the rule followed was move it or block it.
- Ensure that there are no holes or chinks in the telescope or spectrometer boxes which could let in unwanted radiation.

3.6. Contamination control

The use of a near normal incidence diffraction gratings in the 300 to 580Å wavelength range placed severe demands on the gratings' surface cleanliness at the molecular level. In addition, the need for low scatter high reflectivity surfaces for the grazing incidence components placed demands on both molecular and particulate cleanliness. The contamination control of the CDS optics was based on the intrinsically clean design of the optical bench which ensured that optical components were contained in an enclosed volume. The optical bench is shown in Figure 10. The bench could be purged with a constant flow of clean dry nitrogen during instrument assembly, the purge gas being filtered for particulates, water vapour and hydrocarbons. With one or two exceptions, only metals and glasses were enclosed in the optical bench. The exceptions include the lubricant for the slit mechanism for which the sputtered lead film previously mentioned was selected, and the black coating of a thermal control beam stop prior to the entrance slit which used the conducting black paint Electrodag 501 (see section 6).

In order to limit the contamination arising from components of the instrument itself, a comprehensive cleaning programme was undertaken. Different cleaning programmes were applied to different categories of component but with the sole exception of the glass (zerodur) of the optics themselves the final cleaning and verification process of all components consisted of a vacuum bake, at a temperature appropriate to the component in question.

In addition to the thorough cleaning process, a screening programme ensured that only very low outgassing materials were used in the instrument construction. A special ultra-high vacuum system was built and dedicated to surface science diagnostics. In this apparatus material samples selected as low outgassing materials were held at elevated temperature to expel, in a controlled manner, outgas products which were allowed to contaminate previously characterised gold coated witness mirrors. The outgas products were monitored by a quadrupole residual gas analyser and a quartz crystal micro balance. The contaminated witness mirror surfaces were chemically characterised without breaking vacuum using X-ray photoelectron spectroscopy. This system allowed the selection of suitable materials for the wiring harness and components within the multilayer insulation used as part of the thermal control system (Kent *et al.*, 1993, 1994).

During assembly, alignment and test, gold-on-glass witness samples were regularly examined (by X-ray photoelectron spectroscopy) to monitor molec-

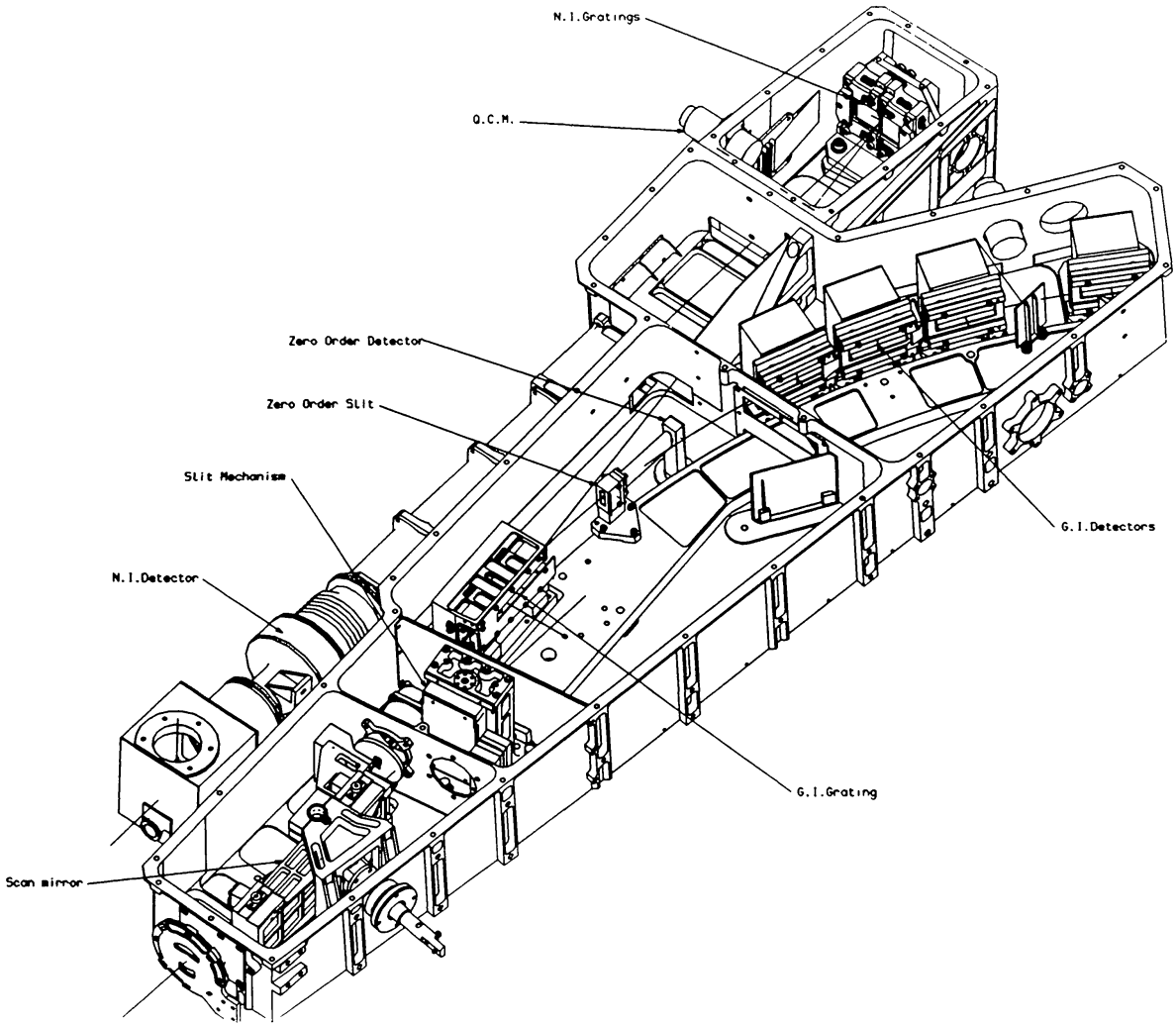

Fig. 10. The CDS Optical Bench, which encloses most of the optical components of the instrument. Light from the telescope enters the bench through the aperture stop at the lower left, which shows two apertures (one for the GIS, one for the NIS).

ular contamination in the instrument and its immediate environment. The entire instrument assembly and test took place in class 100 clean rooms monitored for particulate cleanliness with both on-line air sampling and surface cleanliness sampling by means of particle fall out plates to ensure that class 100 conditions were in fact met.

For in-flight contamination monitoring, two quartz crystal microbalances (QCM) are mounted on the optical bench (see Figure 10).

4. Mechanical Design

All the optical components except the telescope are located in an enclosed optical bench. This enables all the contamination sensitive components to be protected, as well as allowing all the optical components to be aligned as a unit outside of the main structure. The telescope is also contained within its own volume for cleanliness reasons, the two volumes being connected with a tube and flexible bellows arrangement.

The purpose of the main structure is to support these two components in their correct alignment, and provide an interface to the spacecraft structure. A secondary purpose of the main structure is to carry several electronics units plus harnesses and thermal control hardware.

4.1. The main structure

The telescope-spectrometer interface consists of a circular flange at the rear of the two telescope mirrors, hence a substantial bulkhead was required at this location. After studying several designs it was decided that the primary structure should be of an open truss design, manufactured from aluminium alloy using machined sections and bolted joints (Figure 11).

From the telescope bulkhead, two side frames machined from aluminium alloy extend rearwards for most of the length of the instrument. At three positions, bulkheads are attached to provide fixing points for the components and to provide the necessary load paths from one side to the other. The structure is heavily cross braced with diagonal struts between each bulkhead.

A thin wall tube extends forwards from the telescope bulkhead to carry the front Sun shield and aperture door assemblies, as shown in Figure 12. The telescope is contained in the black cylinder behind the sun shield.

4.2. The Optical Bench

The optical bench (Figure 10) houses all spectrometer optical components. The optical paths of the two spectrometers are inclined at an angle of a few degrees to one another. To accomodate this feature, the optical bench is divided into three sections. The front section which is in a horizontal plane houses the scan mirror and the slit assembly, the centre section contains all the grazing incidence components and is inclined upwards. The normal

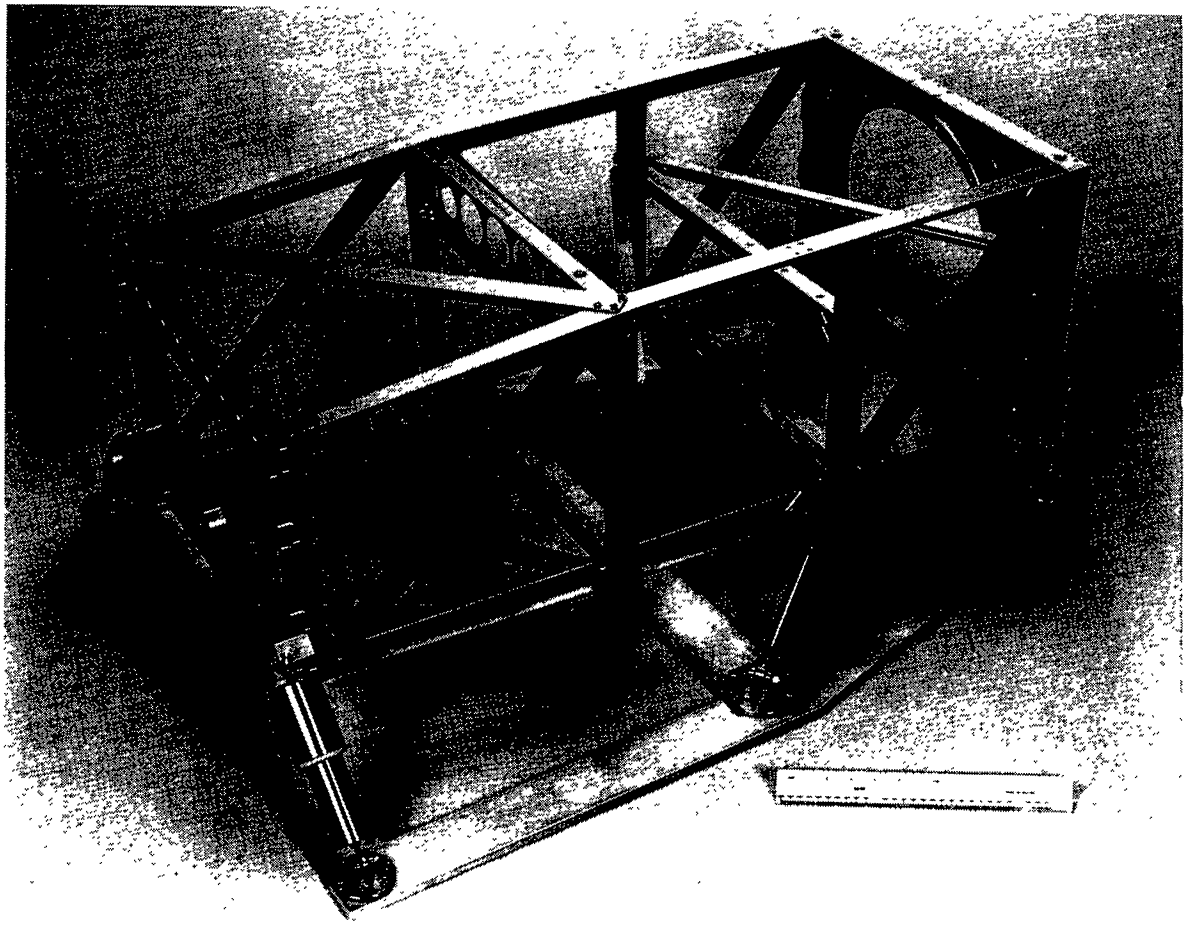

Fig. 11. The main structure, consisting of an open truss design in aluminium alloy, shown with the telescope bulkhead to the right.

incidence gratings are housed in a section which is bolted to the rear of the bench and the VDS is attached to the side next to the scan mirror. In order to obtain the required accuracy and stability the main section of the bench was machined from a single piece of aluminium alloy.

Figure 12 shows the complete flight system, the optical bench lying at the heart of the main structure. The rear of the optical bench, which encloses the NIS gratings, is clearly visible, as is the tubular light path to the VDS detector.

To be able to align the optical components in the optical bench and then install the bench within the structure without compromising this alignment, an isostatic mount was necessary. The design is a conventional three point mounting using spherical joints incorporated into thin blade mounts which allow thermal expansion or contraction to take place without distorting the optical bench.

To keep the load paths as short as possible, these three mounting points are positioned on the bulkheads to which the main support links are attached.

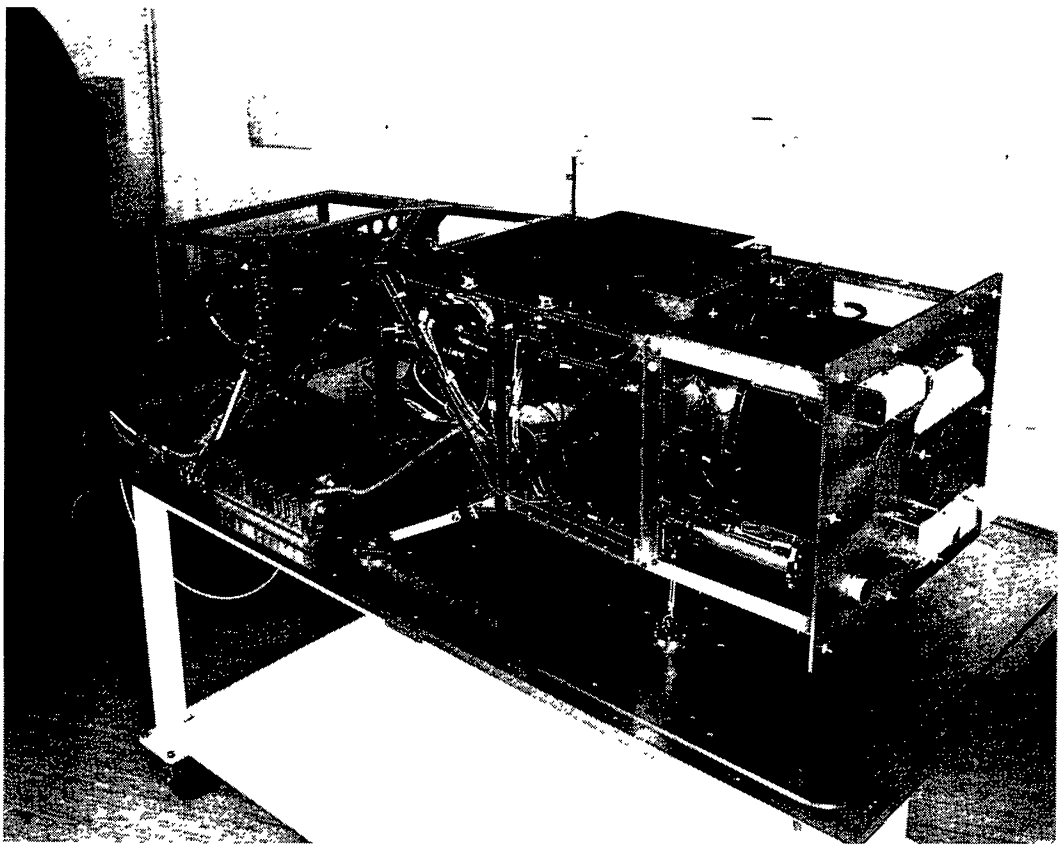

Fig. 12. The CDS flight model (see text)

Two are positioned on the rear bulkhead close to the actuators and the third one on the bulkhead to which the central angled links are attached.

4.3. Analysis

A 400 node, 500 element model was constructed. The framework was modelled using linear beam elements, the bulkheads were modelled using quadrilateral plate elements and the support links were treated as rod elements, which cannot take bending loads. The non structural components such as electronics units were modelled using lumped mass elements. After many iterations a final design was reached which fulfilled the launcher requirement of a first natural frequency above 70Hz and was within the mass allocation. However, modal analysis of the structural model instrument indicated a much lower natural frequency. Indications showed this to be caused by the non-linear behaviour of the instrument mounting system. Further development was carried out and a final first natural frequency of 52 Hz was achieved which was accepted by ESA.

In parallel with the structural modelling, detailed thermal modelling was carried out. This analysis defined the position of heaters and temperature

sensors necessary to maintain the temperature of the structure within two degrees of room temperature. It also dictated that titanium alloy would be necessary for the support links and mounting feet to meet the thermal isolation requirements.

4.4. Manufacture

All the detail drawings for the primary structure were produced on the Rutherford Appleton Laboratory (RAL) Medusa computer aided design (CAD) system. The drawing files were then transferred directly to computer numerically controlled (CNC) machines, where the manufacture of the components took place.

All the components were manufactured from aluminium alloy to BS 1470 L115 T651. This is the solution heat treated, artificially aged and controlled stretched version of this alloy, and was used to minimise distortion due to heavy machining. No heat treatment or stress relieving was carried out during or after machining.

4.5. Mechanisms

There are four different mechanisms on CDS, two identical linear actuators, which move the whole instrument, a slit drive mechanism, a scan mirror mechanism, and mechanisms for the two aperture doors.

4.5.1. The Pointing System

The instrument is required to point through $\pm 0.38^{o}$ in two axes and be isostatically mounted to the spacecraft. Many schemes were investigated in order to achieve these requirements, but most solutions had the effect of considerably reducing the first natural frequency of the structure compared with its frequency in the free condition.

To overcome this fundamental limitation it was essential to support the structure at the points of inflection of its first natural resonance. These positions were calculated and found to be close to the telescope bulkhead at one end and at a position approximately one quarter of the length of the instrument from the rear.

To allow pointing and support of the instrument at these positions, six links with hemispherical bearings on each end were employed. Two vertical links were used at the front, a second set of angled links was positioned such that a virtual pivot point was formed on the centre line of the instrument, above the front links. The remaining two links were positioned towards the rear and were inclined to the side frames at forty five degrees. This arrangement formed an isostatic mounting and supported the structure at its points of inflection. The two rear links were replaced by linear actuators to allow the instrument to point through a small angle in two axes. This arrange-

ment is shown clearly in Figure 11. To keep the natural frequency of the instrument high, the joints on the central legs comprise a flexure design.

The linear actuators consist of 200 step, size 23 hollow shaft stepper motors, driving a plain nut and screw assembly of 1 mm pitch. This arrangement gives a step size of 0.005 mm or a 1 arcsecond pointing increment. A plain nut and screw arrangement was chosen because it is compact enough to fit inside a relatively small motor and is of sufficient load carrying capacity to withstand the launch loads of approximately 3 kN. Also, the efficiency is low enough to prevent back-driving under load. All the load is taken by a back-to-back pair of angular contact bearings at one end of the unit, the central bearing only providing radial support. Position readout is provided by a hybrid track potentiometer, this gives sufficient accuracy while allowing a simple readout system to be used. The motors were supplied by Norcroft limited, Pewsey, Wiltshire, England and the transducers by Penny and Giles, Christchurch, Dorset, England. Lubrication is by Bracote 601 low vapour pressure grease on the bearings, screw thread and the potentiometer tracks.

4.5.2. Slit drive mechanism

The GIS is an astigmatic instrument and, as discussed in section 3.3, builds up images by scanning pinhole slits. The slit drive mechanism consists of a 200 step size 13 stepper motor driving a recirculating ball screw assembly. The slit support frame is attached to a carriage supported by a pair of cross roller slideways. Accuracy and repeatability are most important, ideally the slit should be placed within a small fraction of a slit width, the smallest slit being 25 μm. The measured accuracy with which the slit can be positioned is 10% of the smallest slit width. A second function of this mechanism is to select a slit from the range of six available. Positional information is obtained from a 200 step optical rotary encoder combined with a coarse linear encoder to indicate which slit has been selected.

4.5.3. Scan mirror mechanism

The NIS is a stigmatic instrument which uses a long slit. To build up two dimensional images, the image of the Sun is scanned across the entrance slit by the scan mirror. The mirror drive mechanism is very similar to the slit drive mechanism. A ball screw carriage pushes a lever which is attached to the scan mirror housing. The scan mirror housing is supported in a pair of Bendix flex pivots to allow rotation of a few degrees. Both the scan mirror mechanism and the slit drive mechanism use Norcroft stepper motors and encoders supplied by Muirhead, Beckenham, Kent, England. The ball screws are manufactured by Warner in the USA and the cross roller slide ways are made by Schneeberger, Switzerland. Lubrication of the ball screws and slideways is by ion sputtered lead coating applied by ESTL, Risley, Lancashire,

England. The other bearings used are Bartemp which come directly from the manufacturer in the USA with dry film lubrication.

4.5.4. Aperture door mechanisms

For any UV solar viewing instrument, cleanliness is most important as the influence of solar UV radiation on contaminants can seriously degrade optical surfaces. Because of this, aperture doors are fitted to CDS. These will be closed on launch and opened some time into the mission. After that they can be closed when necessary to avoid contamination during attitude corrections, when the spacecraft thrusters are fired. These doors are a very simple design. A magnetic latch holds the door closed against a torsion spring. On command, a current is passed through a coil around the permanent magnet cancelling the magnetic field and allowing the door to be released. Closure is achieved by a size 13 stepper motor attached directly to the motor shaft. A stepper motor was chosen to avoid the necessity for a gear box, or the high starting current associated with DC motors. Magnetic reed switches indicate the door open and closed positions.

5. Electrical Design

The electrical design of CDS is dictated by the highly complex nature of the twin spectrometer system. An overview of the electrical design is given in Figure 13 which indicates the components attached to the optical bench, units mounted on the CDS structure and units mounted on the spacecraft. The heart of the electrical system is the Command and Data Handling System (CDHS) which is a transputer driven facility. A transputer is a fast processor which can be linked to other processors to form a parallel processing network (see e.g. Barron, 1978). The devices used in the CDHS are IMS T805 transputers with 32 bit architecture. The CDHS controls and monitors the various electrical aspects of CDS and handles the data-stream. This unit is mounted on the spacecraft. Also, mounted on the spacecraft is the Experiment Power Supply (EPS). The detectors (NIS and GIS) have dedicated transputer controlled electronic units mounted on the CDS structure, for controlling and monitoring the detector units themselves and for relaying data to the CDHS and interpreting commands from the CDHS. Also mounted on the structure is the Mechanism Control Unit (MCU) which controls the slit and mirror mechanisms, the pointing actuators, the doors and the heaters. Again, this unit responds to command from the CDHS and relays housekeeping data back to the CDHS for relay to the ground. Attached to the optical bench itself are the GIS and VDS detector units, the GIS zero order detector and filaments, used to monitor the GIS detectors (see section 3.4.2), and the Sun sensor.

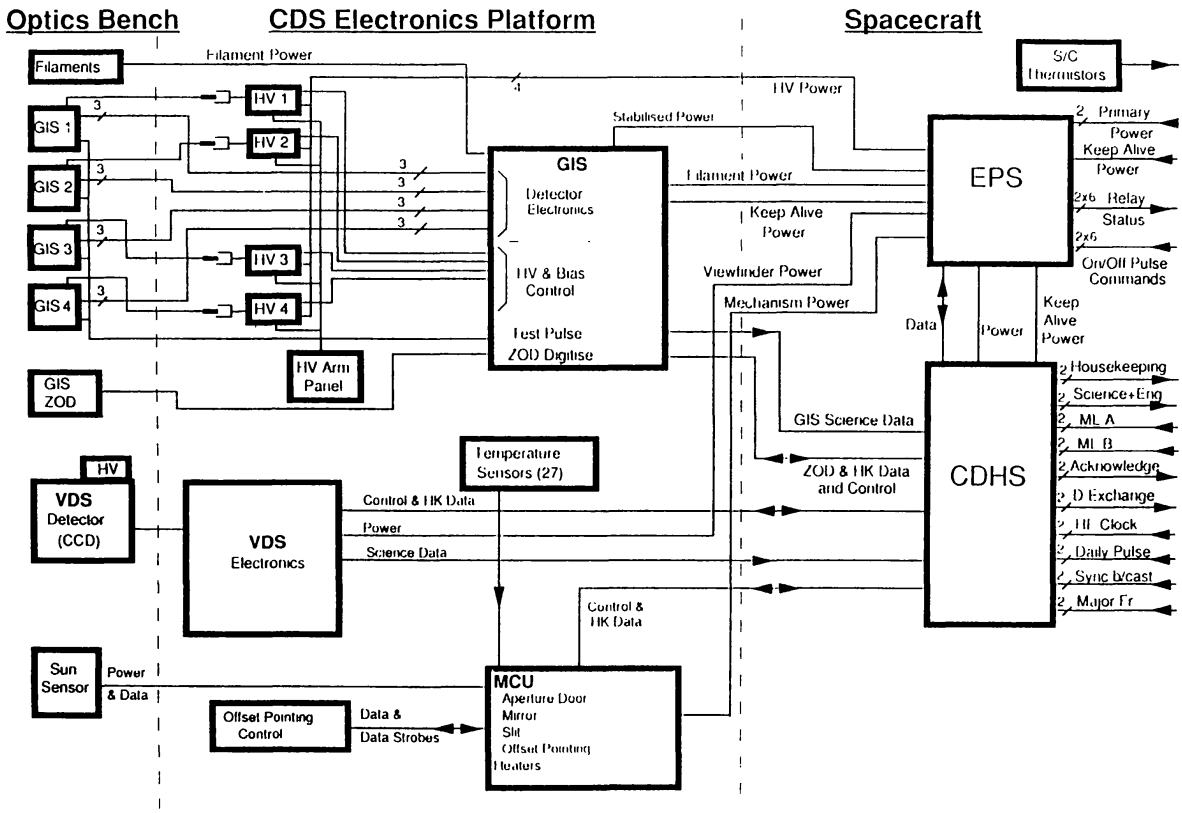

Fig. 13. Overview of the CDS electrical design

Aspects of the electrical design of the detectors and of the CDHS are discussed in other sections. Here, we discuss the MCU and EPS.

5.1. Mechanism Control Unit

The mechanism control unit (MCU) is responsible for controlling all the mechanisms on CDS, for monitoring and controlling the temperatures, and for digitizing the sun sensor and quartz crystal microbalance outputs (which are used to monitor contamination). It incorporates its own power switching and data interfaces with the CDHS.

The mechanism control systems comprise the mirror control system, the slit control system, the offset pointing system, and the door control system. Where stepper motors are used, a novel trapezoidal drive waveform is used, providing a smooth mechanism motion. A fourier analysis of the movement and of vibrations induced showed a substantial improvement over the normal square wave drive.

The MCU interface with the CDHS uses a fully redundant complementary interface. It is designed in such a way that each receiver circuit will continue to function in the event of any wire going open circuit.

The slit and mirror drives incorporate a digital closed loop feedback system, using a 200 step optically coupled absolute encoder. To guard against component failures, an independent single step system is included in each system, using a different set of components. Operation is possible even in the event of the complete failure of the closed loop system. The slit control system differs from the mirror control system in that it also includes slit selection logic.

Control of the offset pointing system (OPS) similarly incorporates independent single step and closed loop modes for reliability. The OPS system uses linear potentiometers as feedback elements rather than optical encoders, and measures mechanism position rather than shaft rotation. A backup potentiometer provides redundant telemetry information. The OPS control system has the disadvantage that it will always tend to overshoot by one step, i.e. $\sim$ 1 arcsecond, but cannot oscillate.

The door control operates the magnetic latch which opens the door, and the stepper motor which closes it. A number of backup modes are included.

The 32 temperature sensors are connected in a matrix arrangement, minimizing the number of interconnections and the amount of wiring. Each one is digitized to 12 bits, i.e. 0.125 degree Kelvin. Temperatures are obtained on request by the CDHS. The heater control system controls the 16 main heaters and 8 backup ones. The main heaters are each thermostatically controlled to follow its nearest temperature sensor. The backup heaters are switched by a data word from the CDHS. In addition to following its temperature sensor, the prime heaters are subject to power level control.

The Sun sensor system digitizes the pitch, yaw and Sun-presence voltages to 12 bits, giving an accuracy of order 10 arcseconds.

The quartz crystal microbalance (QCM) system telemeters the operating frequency and temperature of the QCM crystals.

5.2. Experiment Power Supply

The Experiment Power Supply (EPS) performs a number of functions vital to the operation of the CDS experiment.

The EPS is powered by 2 dual redundant +27 V DC power feeds from the spacecraft. The power interface used is determined by a spacecraft controlled relay within the EPS. In addition the spacecraft supplies prime and redundant "keep-alive" power lines. These lines are regulated by the EPS and used to supply power to CDHS and GIS memories which store critical information. There is dual redundant, bi-directional communication link between the EPS and CDHS. The link is used for instrument level control such as the switching of power to other subsystems and instrument housekeeping.

Contained within the EPS is the switch mode DC-DC converter supplied by MBB, Munich. This provides 3 output rails, generated from the main spacecraft bus, one controlled (+5 V rail) via an isolation amplifier and 2

outputs (+/- 12 V) post-regulated with series regulators. In addition the converter performs input/output isolation and filtering, secondary current limitation and protection against bus over/under voltages, secondary over voltages and short circuit overloads. The regulated outputs from the converter are switched to instrument subsystems using relays controlled by the CDHS. The inputs to various system critical supplies is via other relays controlled by the spacecraft. In addition, the EPS supplies, via relays, a direct +27 V supply, to tolerant loads such as heaters, high voltage supplies and electro-mechanical mechanisms.

The two filaments, housed in the GI spectrometer, are supplied by a controllable constant current source within the EPS. Power switching to the filament ensures only one is active at any one time.

House keeping data providing information concerning input and output voltages and currents, relay status and temperature measurements is assembled in a table which can be read by the CDHS.

6. Thermal Design

The instrumental performance, which is driven by the scientific objectives of the experiment, places a number of requirements on the thermal design of CDS, namely:

- Structure and optical bench - maintain at 20°C with temperature gradients not exceeding 2°C;
- power budget - operational heater power budget nominally 12 W;
- spacecraft interface - conductive exchange less than 1.5 W;
- CCD detector - operational temperature -70°C;
- multilayer insulation - external layer electrically conductive, non-specular and unperforated;
- optics - prevent excessive temperatures in telescope, scan mirror and slit;
- thermal hardware - compatible with cleanliness requirements of CDS;
- survival heaters - power requirements not to exceed 50 W.

These requirements have resulted in a thermal design comprising both passive and active control elements.

Since the ground assembly and calibration temperature was $\sim$ 20°C the mean instrument structure temperature is controlled to 20°C. Furthermore the thermal gradients within the structure and optical bench must be less than 2°C in order to prevent distortions. These two requirements are met by the careful positioning of sixteen operational heater circuits each comprising of a calibrated temperature sensor and a kapton thermofoil heater. Each temperature sensor is sampled by the MCU 8 times a second and the associated heater switched according to some simple on-off control laws. The set point for each circuit is nominally set to 20°C but may be changed by

ground command if required. Control bandwidths of +/- 0.1°C have been maintained using this method.

Although the structure and optical bench are manufactured from a high conductivity aluminium alloy, temperature gradients of less than 2°C could be maintained with the levels of heat dissipation associated with some of the electronics boxes and the incident solar radiation. For this reason an early decision was made to thermally decouple these sources within structural limitations and reject their heat directly to space. Hence the electronics platform is mounted to the structure using titanium alloy screws and delrin spacers. The tops of the four electronics boxes on this platform are painted with a conductive black paint (Electrodag +501) and are partially exposed to space for heat rejection. This produces a platform temperature of about 20°C under operational conditions resulting in a low level of heat exchange with the structure. The temperature controlled heaters on adjacent bulkheads ensure that leakage into the platform does not result in local thermal gradients within the structure. The sidewalls of the four electronics boxes are also painted black to increase radiative coupling and minimise gradients within the platform itself.

The solar energy entering through the two instrument apertures amounts to about 19 W, half of which is absorbed by the gold-coated telescope mirrors and radiated back through the apertures to space or conducted through an invar support tube. From here it is conducted along the black painted forebody towards the front panel and radiated to space from the telescope radiator, an exposed section of the forebody which has a good space view.

The solar power which is not trapped by the telescope continues into the optical bench via a stainless steel bellows which acts as a light-tight contamination shield. On entering the optical bench it encounters the first thermal stop which absorbs unnecessary components of the beam and therefore reduces the incident flux on the scan mirror to tolerable levels. The scan mirror and its mount absorb up to 1 W and reflect the rest onto the second thermal stop which absorbs the remaining unnecessary components of the beam and admits to the slit only about 0.2 W of solar power. Both thermal stops are constructed from aluminium alloy and are painted with Electrodag +501 black paint on the illuminated surfaces and polished to a mirror finish on the non-illuminated surfaces. Each stop is decoupled from the bench using a titanium alloy mount and is conductively coupled to the radiator on the side of the instrument using a flexible aluminium heat strap to reject the high power density solar loads safely to space.

To ensure that positive control margins are maintained for the four operational heaters on the optical bench the lower surface of the bench (onto which the heaters are bonded) is painted black. The remaining surfaces of the bench, in common with those of the main structure, are left as plain alochrom. The instrument is covered with MLI (Multi-Layer Insulation)

having an effective emissivity of 0.02. It is constructed from eighteen core layers comprising perforated double aluminised mylar radiation shields with Dacron net spacers plus an additional four crinkled Kapton radiation shields adjacent to the external layer. The external layer, with the exception of the Sun-facing surface, is black kapton having been chosen mainly to meet the requirements on non-specularity and electrical resistivity laid down in the spacecraft interface document. The front panel MLI external layer is indium-tin-oxide coated aluminised kapton and has 36 core layers to reduce the solar load entering the front panel. All external MLI layers are non-perforated which forces venting of the instrument to occur mainly through a specifically designed vent hole at the rear of the instrument. This enables a more controlled flow of gases to reduce the risk of inter-instrument contamination. The blankets are made as large as possible within handling constraints to reduce the number of sharp edges which reduce thermal performance.

A major thermal design challenge was provided by the VDS detector which requires an operational temperature of less than -80°C to limit dark current to acceptable levels. This temperature is achieved using a radiator having an area of 1534 cm^2 mounted on the top surface of the instrument and having a view factor of almost unity to deep space. It is decoupled from the structure using carefully designed delrin legs and is coupled to the detector with a baffled and polished aluminium cold finger incorporating a flexible coupling at the detector end to reduce dynamic loads.

The aluminium aperture doors present a particular problem since one side of each door is always facing the Sun whether it is open or closed. When closed the doors also view the telescope optics and without careful design contamination products could be released and deposited on these sensitive optical components. Both sides have been coated white (Plasmocer from PTS, Jena, Germany) which was found to have relatively good thermal performance with an exceptionally low contamination risk.

The instrument must not exchange more than 1.5 W by conduction with the spacecraft and is therefore thermally decoupled from the spacecraft payload panel using titanium alloy fixed legs and fittings. The rose bearings (two per leg) also greatly assist in conductively isolating the instrument from the spacecraft - the largest single conductive exchange is, in fact, along the electrical harness.

The overall power budget for CDS is 58 W and the nominal allocation for the operational heaters is 12 W although under some instances this may be more if the electronics boxes are running at a lower power level. The thermal design discussed above meets the various requirements within this power budget although in general the problem has been to maintain thermal control margins in the hot cases but to remain within the budget under cold cases.

During non-operational phases of the mission survival heater power is supplied directly to CDS from the spacecraft. The survival heaters are of a similar type to the operational heaters and are distributed as a single circuit around the instrument to minimise temperature gradients. The maximum available power delivered by these heaters is 50 W.

7. Instrument Commanding and Data Handling

The CDS on-board processor hardware, called the Command and Data Handling System (CDHS), consists of one or two operating transputers (CPU's), one standby transputer, memory, and subsystem interfaces. For convenience the two operating CPUs are here referred to as "primary" and "secondary", and the standby CPU as "redundant". These CPUs are interchangeable. The CDHS hardware was developed by Satellites International Limited, Newbury, England.

The CDHS software and CDS hardware operate in a series of specific modes controlled by the CDHS program. Each mode defines a specific status for each instrument system; the commands required to set up these modes are stored in the CDHS memory. Mode switching is achieved by sending a single command to execute the mode table. This command can be sent either in real time or time tagged (stored in the CDHS rather than in the spacecraft computer).

The diagram in Figure 14 shows a basic interpretation of the modes and transitions for the CDHS. In Table IX, we summarise the state of some of the CDS subsystems in each mode.

The bootstrap is the first program loaded on the system when it is switched on. It runs on the primary CPU, which can be selected by ground command to be any of the three processors. The program is loaded and run automatically and resides in PROM. The bootstrap program checks the contents of the RAM, and if correct, runs the main program residing in the RAM. If the RAM is corrupted, it automatically loads the main program from EPROM. It is possible to switch the bootstrap program into patch mode, in which case individual program modules can be loaded from the command stream, i.e. from the ground.

Once loaded and running, the main program will control all the subsystems, keep them within operating limits, transmit data and receive commands, and operate autonomously when not in ground control. It would be usual to enable one of the other CPUs as the secondary. Once enabled, the science modules from the main program are copied to it, and run. The science modules look after the collection and compression of the science data.

If one CPU fails, then the system will reboot into ZZZ mode, and then after five minutes into SBY mode. The program will then wait for recovery commands from the ground. If the failure is irrecoverable, the redundant

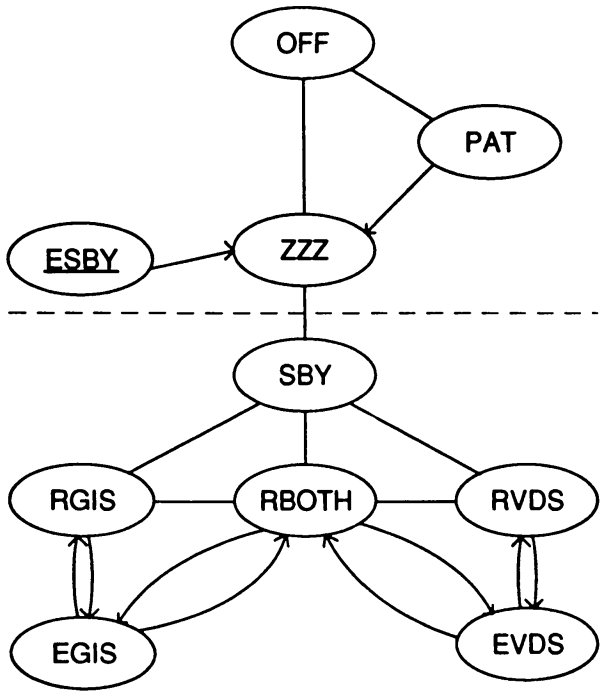

Fig. 14. CDS CDHS Modes. Mode transitions can only follow the lines indicated, except transitions to emergency standby (ESBY). This can be reached from SBY, all RDY and all EXE modes. Transitions above the dashed line must be commanded from the spacecraft (from ground); transitions below the line can be commanded either from ground or automatically from a deferred command store.

CPU can be switched on and used instead. If two CPUs fail, it is possible to run the primary processor program and the science modules on the remaining processor, although the amount of science data transmitted to the ground could be limited.

A single CDS observation consists of a 'raster' of slit and mirror movements with an exposure and data collection at each position. The observation is controlled by a series of commands stored in a sequence table. The commands control also the detector settings, the location or position of the raster and the data selection and compression parameters. The observation is initiated by a command to run the sequence table. This command may be given from the ground or from a deferred (time tagged) command store.

Due to the limited spacecraft resources it is not generally possible to have both the GIS and NIS systems operating simultaneously, i.e. operating an EXE mode at the same time. This poses some difficulties for observations that require rapid switching from one spectrometer to the other and a small time allowance must be included to allow for this.

The operational lifetime of the high voltage supplies depends on the number of on/off cycles they experience. Accordingly, transitions are not allowed if they occur faster than one every 5 minutes or more frequently than 150

TABLE IX
CDS Mode Summary

OFF	Experiment off. Spacecraft survival heaters on. Doors closed. No telemetry.
ZZZ	Snooze mode - All subsystems off (except CPU & spacecraft interface). Doors closed. Basic housekeeping telemetry transmitted. Spacecraft survival heaters on. Switches to SBY mode after 5 min unless 2nd ZZZ command sent.
SBY	Standby mode - Full safety checks performed, e.g. high voltages off. Door opened. Thermal control maintained internally. Full CDHS software check made. Normal housekeeping/engineering telemetry restarted.
ESBY	Emergency Standby mode - similar to SBY. Entered from any mode except OFF, ZZZ and PAT. CDHS can issue ESBY command when a problem is, detected or the spacecraft computer can send it (automatically or from the ground). If ESBY is entered due to a spacecraft emergency, the doors are closed.
PAT	Patch mode - used to overwrite whole modules of on-board code. To avoid overwriting running code, no other processing can take place while in PAT. Note - very small patches (a few bytes) and scientific or engineering sequence changes can be loaded while in most other modes.
RDY	In all the Ready and Execute modes mentioned below, one or other detector systems and the mechanisms are enabled: RGIS - Ready GIS - GIS subsystem enabled - high voltage power units on RVDS - Ready VDS - VDS subsystem enabled - high voltage power unit on RBOTH - Ready Both - GIS/VDS subsystems enabled - high voltage power units on. RBOTH can only be used if sufficient spacecraft power available.
EXE	Execute mode - CDHS automatically executes a pre-defined scientific or engineering sequence. The system will drop back into the relevant RDY mode when the sequence is complete.

cycles per week. Note that alternating between ready and execute mode for the same spectrometer does not switch the high voltage on and off.

The CDHS monitors all of the important instrument parameters and takes appropriate action as necessary. The intention is that the CDHS program will not attempt to correct any malfunction or deviation, but it will put the instrument into a safe mode until the next real time contact from the ground.

Apart from some power and configuration commands, all other CDS commands are sent directly to the CDHS. Commands may be for immediate execution or time tagged for later execution. An array of time tagged commands is called a timeline and this is the method by which the instrument will be operated when the spacecraft is not in contact with the ground. Before use, stored commands must have been demonstrated to operate correctly and safely during real time operations. The command sequences will be uplinked and stored in an onboard deferred command store ready to operate at the appropriate time.

If an "interesting" event occurs on the Sun, it is possible to send automatically the event's solar coordinates to other instruments. If enabled to receive such data, the CDHS will command the mirror and slit mechanisms, and, in some cases, the pointing system, to the relevant coordinates and look at the event. If enabled to send data, the CDHS will look for interesting events, and if found will transmit the coordinates to the other instruments.

At least two engineering packets and one housekeeping packet are telemetered every $\sim$ 15 s. Thus the minimum engineering data rate is 19.6 16-bit words per second and the housekeeping rate is 6.3 16-bit words per second.

The last 16 bit word in all CDS telemetry packets contains a checksum, to provide a means of monitoring the receipt of data. This checksum is the 'exclusive OR' of all the words in the packet (except the last 16 bits) as generated by the CDHS.

The CDHS receives command blocks containing up to 32 16 bit words. It will translate the commands (if necessary) and pass them on to the relevant subsystem. To accommodate all the different command schemes for the subsystems, each command block contains a header (the first command word), which specifies the number of 16 bit words in the block, and the subsystem for which the commands are intended.

In common with many of the instruments on board SOHO, CDS is able to produce data at a far higher rate than it can be transmitted or stored. The CDHS is capable of compressing and storing data before delivery to the spacecraft telemetry system. This telemetry system will operate with four formats; the prime format allows an equitable allocation for all the instruments, while the other three allow different instruments to take advantage of a higher rate of transmission. This includes a CDS high data-rate. The times for telemetry format switching will be planned during the normal planning procedures, generally being fixed during weekly planning meetings. The telemetry rates are summarised in Table X.

8. Calibration and Performance

The CDS scientific program has as its goal the measurement of accurate spectral line intensities, both relatively and absolutely, in order to apply

TABLE X
CDS Telemetry Rates

Sub mode 1	Normal operations	11.3 kbit/s
Sub mode 2	EIT prime	1.9 kbit/s
Sub mode 3	CDS prime	22.6 kbit/s
Sub mode 4	SUMER prime	1.9 kbit/s

established techniques to derive diagnostic information on the plasmas of the solar atmosphere. Absolute intensities and intensity ratios can be used to obtain information on abundances, density and temperature. Such information can be obtained only with an accurate knowledge of the instrument sensitivity and performance.

Good intensity calibration being central to the instrument design concept, the CDS team have instigated a thorough pre-launch calibration program, and have developed in-flight calibration and monitoring schemes. A transfer source, calibrated against synchrotron radiation, is used to provide a pre-launch absolute spectral intensity calibration. For each calibration activity, the transfer source was calibrated against the BESSY electron storage ring, in Berlin, and transported to the Rutherford Appleton Laboratory. There, the source was used to illuminate the CDS instrument to achieve an end to end calibration. Then, the source was returned to Berlin for post-calibration checks.

The transfer source is a high-current hollow cathode discharge lamp which emits intense unpolarized line radiation from a buffer gas and the cathode material (99.5% aluminium) at wavelengths longer than 130 Å. Equipped with a compact two stage differential pumping system, the hollow cathode source allows windowless observation of its radiation under ultrahigh-vacuum conditions. The source has been optimised to operate as a radiometric standard of radiant intensity. A detailed description of its operation and radiometric characterisation is given by Hollandt *et al.* (1993, 1994).

The transfer source incorporates a reverse-illuminated Wolter-Schwarzchild type 2 grazing incidence telescope, to produce parallel radiation. An aperture on the CDS side of the collimating telescope limits the collimated beam to 5 mm diameter. The complete source/collimator assembly is mounted on a platform that provides a precise vertical movement.

For the sensitivity calibration of CDS twenty-five emission lines from the calibration source were selected, which cover the full spectral range of the instrument. The photon flux of these emission lines has been determined by comparison with the spectral photon flux of the electron storage ring BESSY. The storage ring is a primary radiometric standard source since

the spectral photon flux of the synchrotron radiation can be calculated from the knowledge of the storage ring parameters (Riehle *et al.*, 1985, Arnold *et al.*, 1994).

In the spectral range from 160 Å to 600 Å the calibration of the CDS calibration source was performed with a toroidal grating monochromator beamline at BESSY (Fischer *et al.* 1986). To allow the comparison of the transfer source with the synchrotron radiation an ellipsoidal focusing mirror was included which could image either the tangent point of the storage ring or the aperture stop of the transfer source into the entrance slit of the monochromator, in such a way that the entrance slit was not limiting the photon flux. The monochromator could be moved along its optical axis to maintain focus and compensate for the different distances of the two sources. To allow for corrections due to the different degree of polarisation of the transfer source and the synchrotron radiation the monochromator could be rotated by 90° around its optical axis, defined by the centre of the grating and the entrance slit.

In the spectral range from 400 Å to 800 Å a normal incidence monochromator beamline (Hollandt *et al.*, 1992), based on a spherical imaging mirror and a 15° McPherson type monochromator, was used to complete the calibration. The whole instrumentation could be rotated around a vertical axis, allowing the spherical mirror to form alternatively an image of the tangent point of the storage ring or the aperture stop of the hollow cathode source in the entrance slit of the monochromator. Again the monochromator could be rotated around the optical axis to allow for corrections due to the different degree of polarisation of the two sources.

The photon flux in a range of EUV emission lines of the source beam has been established to be in the range 10^4 to 10^8 photons/s and is comparable to the accepted solar flux of CDS. The relative uncertainty of the measurement of the source photon flux is between 6% and 8% (1 sigma confidence level). The specific calibration source emission lines, their associated uncertainty and the contributions to that uncertainty are given by Harrison *et al.* (1995).

The pre-delivery CDS flight instrument calibration activity took place in a four week period during February and March '94. The CDS instrument was mounted on a precision translation table inside a stainless steel vacuum tank, which was evacuated to a pressure of $2\text{x}10^{-6}$ torr. The source was coupled to the instrument tank by means of a turbo pumped beam pipe providing an additional differential pumping stage so that the high gas pressures present in the source did not influence the instrument vacuum chamber.

Since the calibration source could not fully irradiate the primary telescope mirror of CDS, the source support platform could be moved so that the 5mm diameter collimated source beam moved across the CDS aperture parallel to the entrance slits and by movement of the translation table inside the vacuum chamber CDS could be tracked across the stationary source beam.

Combinations of these two movements thus allowed complete mapping of each of the telescope entrance apertures.

All of the instrument data flowed through the telemetry channel via the instrument CDHS and thus the calibration exercise provided an opportunity for a complete instrument/system end-to-end verification. Below, we describe a selection of the results of the calibration activities. A full report is beyond the scope of this paper but will appear in the open literature in due course.

8.1. Wavelength calibration

The known wavelengths of the emission lines from the ionised gas in the radiation output from the hollow cathode source provide a convenient wavelength calibration for the CDS instrument. Spectra for each of the GIS detectors are shown in Figure 15 and for the NIS in Figure 16.

The GIS data were recorded as a one-dimensional arrays - 2048 for each detector. The positions of a number of lines were determined, on each detector, by fitting Gaussian profiles to the data. The relationship between these positions and their corresponding wavelengths was determined by a least-squares straight-line fit. Hence the observed wavelength ranges were determined and shown in Table V for data taken with the 4 x 240 arcsecond slit. Results from the other slits for detectors GI3 and GI4 showed a variation in the end-points of the ranges of less than 1Å between the 2 x 2 and 4 x 240 arcsecond slits.

For the NIS VDS detector, windows on the CCD were selected which either contained the whole spectral range for each detector (NI1 or NI2) or, in some cases, two or three smaller windows around the lines of interest. The full spectral range covered nominally 1024 pixels per detector and the spatial window recorded was usually 140 pixels.

The VDS CCD will be run cool in space but was near room temperature during the calibration which generated a high thermal background. This background, in most cases, swamped the spectra of interest. However, the background was repeatable so for each type of data set a background file was produced by running the integration without any signal. This could then be subtracted from the data file to reveal the spectrum.

When determining line positions, usually the background-subtracted spectrum at the peak spatial position was examined and the centroids determined. The dispersion and ranges were then found as for the GIS detectors. For some weak lines, the data were first integrated spatially to produce a cleaner spectrum. The resulting wavelength ranges are also given in Table V.

The CDS calibrated wavelength ranges are within a few Å of the target ranges and thus, all emission lines of prime interest to the CDS experiment are covered.

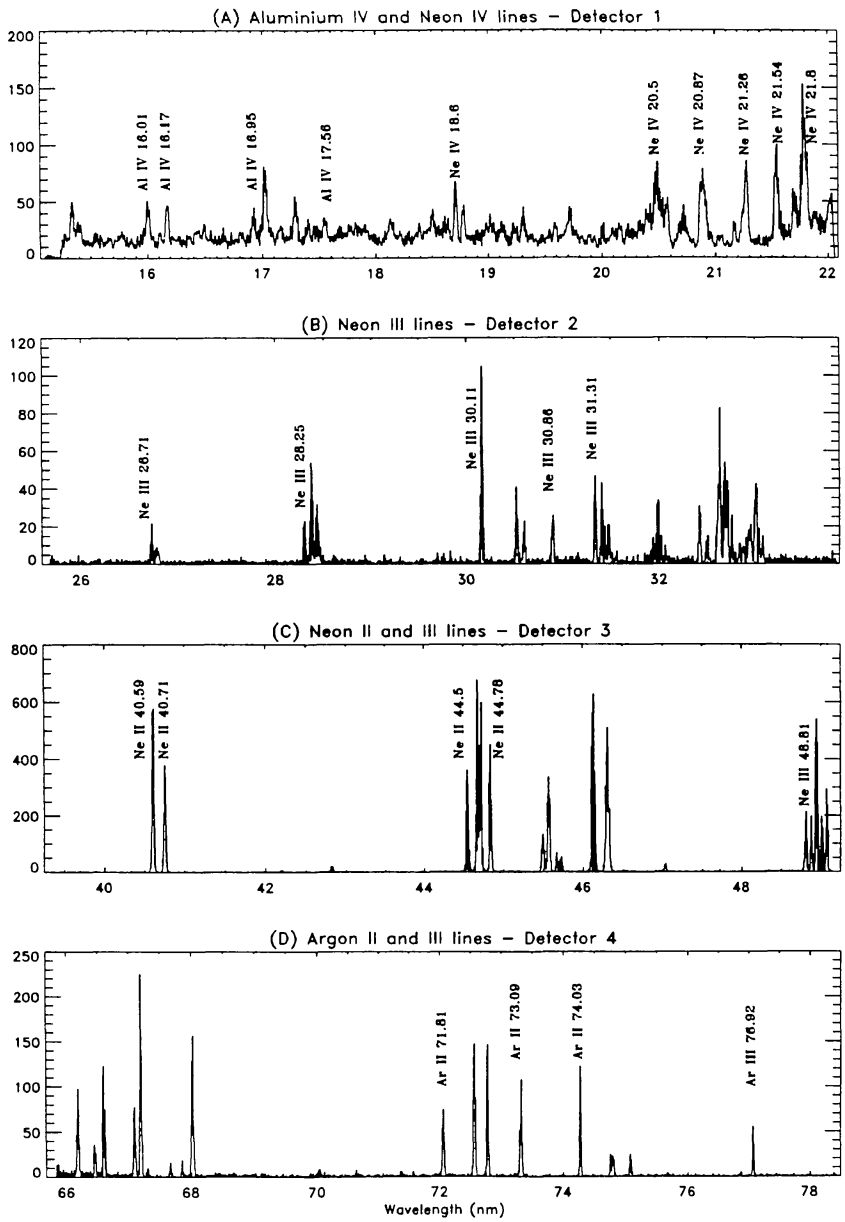

Fig. 15. Example of the GIS calibration spectra. Some neon, aluminium and argon lines are indicated in the four detector ranges.

8.2. Photometric Sensitivity

Given the complexity of the aperture scanning procedure, which involved the mapping of the calibration source beam across the two CDS apertures with the use of multiple slits and different hollow cathode gases, the analysis of the calibration data is a long drawn out process. It is is well underway, but not complete at the time of writing, and will be the subject of a future dedicated report.

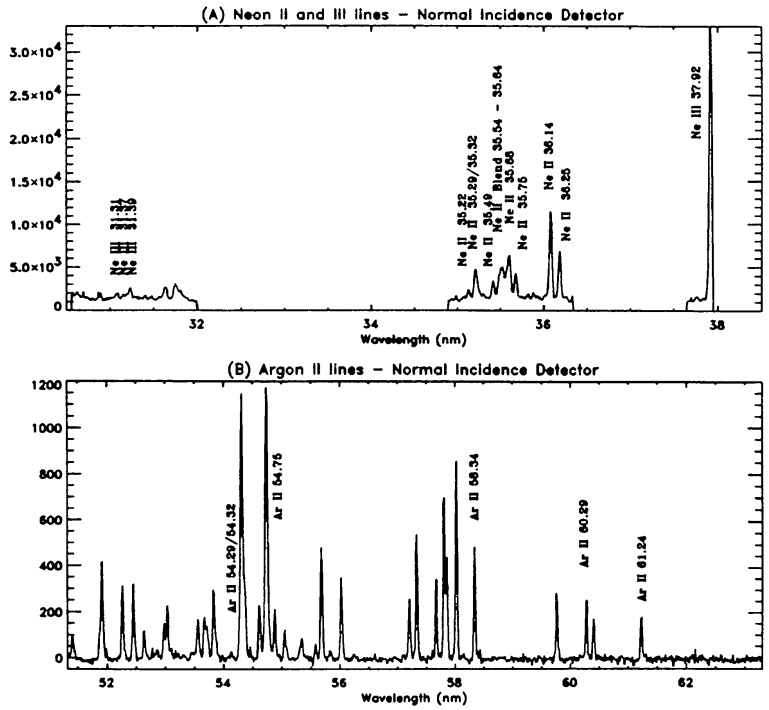

Fig. 16. Example of the NIS calibration spectra. Some neon and argon lines are indicated. In the upper spectrum an example of data windowing is shown, where three bands in the detector range have been selected.

For a given solar emission line intensity, I erg.cm^{-2}s^{-1}ster^{-1}, we may convert to photons by dividing by hc/λ, where h is Planck's constant and λ is the wavelength of the line. For a given slit, we would be examining a specific portion of the solar surface which can be expressed as (abR^2/f^2) by similar triangles, where a and b are the dimensions of the slit (cm), f is the telescope effective focal length and R is the distance to the Sun. So, the intensity at the front of CDS, in photon.s^{-1}ster^{-1} is $(I\lambda/hc)(abR^2/f^2)$. The solid angle is the area available at the telescope, A, divided by R^2. Finally, we multiply by the reflectances and efficiencies of the telescope, scan mirror, grating and detector $(\epsilon_t, \epsilon_m, \epsilon_g, \epsilon_d)$. Thus, the CDS count rate (counts per second) is given by

$$\frac{I\lambda abA\epsilon_t\epsilon_m\epsilon_g\epsilon_d}{hcf^2}.$$

Taking out the geometrical factors, this aspect of the calibration is an attempt to measure the product $\epsilon_t\epsilon_m\epsilon_g\epsilon_d$, the efficiency product. This will not only be a function of wavelength but also a function of angles of incidence, governed by such things as the scan mirror position and the source off-set angle with respect to the telescope axis. Thus, the efficiency product cannot be thoroughly represented by a simple plot against wavelength, and a full discussion is beyond the scope of this paper. A full report will be published. However, as a sample of the results obtained, for observations made

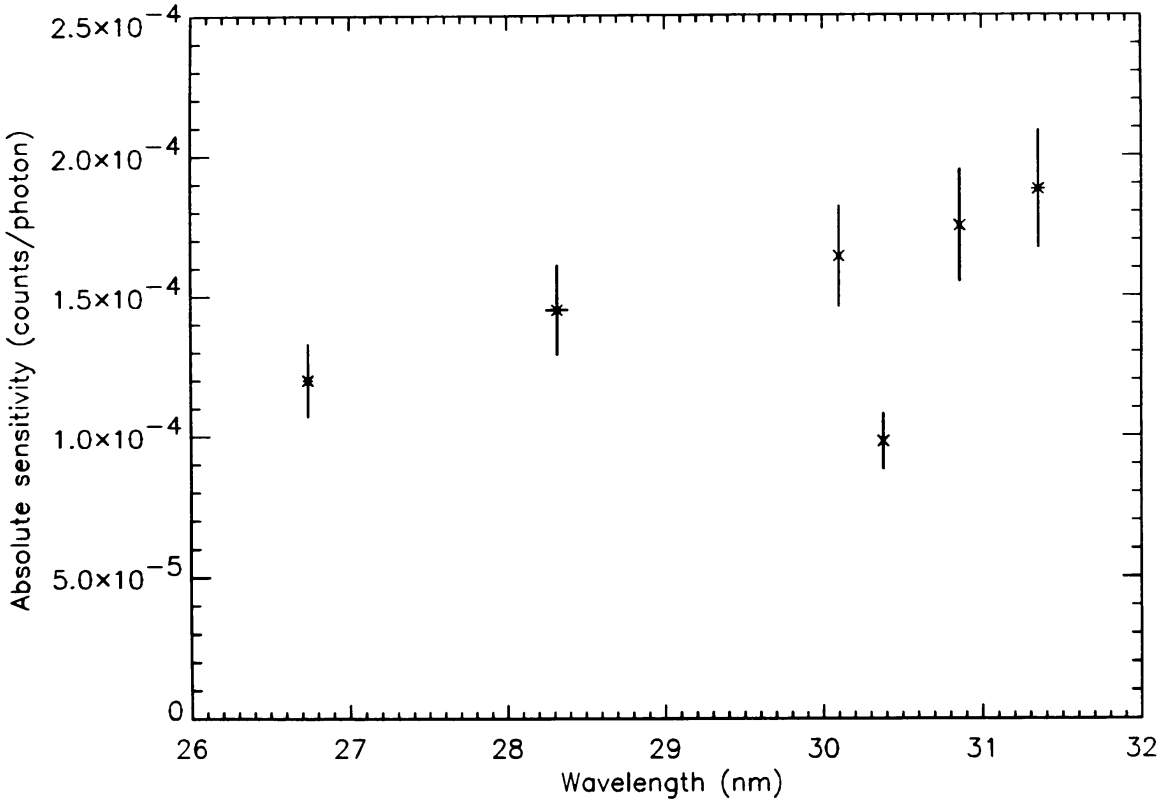

Fig. 17. A plot of the sensitivity (efficiency product) of the second GIS detector as a function of wavelength

on-axis, with the scan mirror in its central position, the efficiency product for the second GIS detector was found to lie in the range 1-2 x 10^{-4}. Figure 16 shows the results for this wavelength range. Given pre-build estimates of telescope, scan mirror, grating and detector efficiencies of 0.25, 0.80, 0.03 and 0.1, for this detector, we predicted an efficiency product of order 6 x 10^{-4}, recognising that this figure was rather optimistic. Thus, the measured to predicted intensity ratio appears to be of order 20-30%, for this particular range, which is an encouraging result. Similar efficiencies for the other three GIS detectors have been established.

In Table XI, we list a selection of emission lines and their expected intensities (for a 2 x 2 arcsecond portion of the Sun). These intensities are projected from solar observations reported by Vernazza and Reeves (1978) and Malinovsky and Heroux (1973). Even with a complete calibration analysis, we would be unable to predict accurate solar intensities for many lines since past EUV instrumentation has been either inappropriate for the estimation of intensities for CDS or instruments have recorded wildly differing values. Furthermore, since past instruments clearly did not have the resolutions available to CDS, the intensities are necessarily spatially averaged; the solar EUV emission may be highly mottled, producing regions of much higher

TABLE XI

Expected count-rates for a number of emission lines. Counts are given per 2x2 arcsec per second for quiet Sun.

Ion	Wavelength (Å)	Intensity	Detector
Fe IX	171.07	5.3	GIS1
Fe X	174.53	5.3	GIS1
Fe X	177.24	3.2	GIS1
Fe XI	180.40	5.9	GIS1
Fe XI	188.22	4.9	GIS1
Fe XII	193.51	4.2	GIS1
Fe XII	195.12	6.2	GIS1
Fe XIV	211.32	5.0	GIS1
Fe XV	284.16	90.5	GIS2
He II	303.78	89.6	GIS2
Fe XIV	334.17	4.7	GIS2/NIS1
Mg IX	368.06	8.9	NIS1
S XIV	417.60	2.4	GIS3
Ne VII	465.22	2.7	GIS3
He I	537.03	3.6	NIS2
O IV	554.52	24.9	NIS2
He I	584.33	30.0	NIS2
O V	629.73	14.9	NIS2
O III	702.98	1.6	GIS4
Ne VIII	770.40	1.7	GIS4

intensities and lower intensities than those listed in Table XI. So, in general, the figures given in Table XI provide a useful guide, but should be treated with some care at this stage.

8.2.1. In-flight calibration

A thorough in-flight calibration and monitoring programme has been designed for the CDS operations phase. These include:

(i) Regular monitoring of quiet Sun intensities and invariant line intensity ratios to determine the variation of the CDS sensitivity with time during the mission,

(ii) The operation of cross-calibration sequences utilising simultaneous or near-simultaneous observations of common wavelength ranges between GIS and NIS as well as between CDS and other SOHO instruments, to provide an understanding of the relative sensitivities of the different spectrometers,

(iii) A cross-calibration using an EUV rocket flight, possibly twice during the mission. This involves the SERTS (Solar EUV Rocket Telescope and Spectrograph) rocket which is operated by a consortium led by the Goddard Space Flight Center, USA (Neupert *et al.* 1992). SERTS will be calibrated in exactly the same way as CDS was prior to and after each flight, and, during the flight CDS will be operated in a complementary mode.

9. CDS Ground Segment

Since SOHO is to be stationed at the L1 Lagrangian point, data will be downlinked via the NASA Deep Space Network for onward transmission to the SOHO Experiment Operations Facility (EOF) at Goddard Space Flight Center. The EOF consists of an array of instrument workstation systems, one of which will be dedicated to the CDS operation and will be permanently manned by CDS staff.

The CDS EOF staff are responsible for implementing the CDS operations through the generation and uplinking of commands and for the acquisition and archiving of incoming CDS data. The CDS EOF workstation will automatically monitor the status and health of the instrument and provide reports to the CDS staff. There will be three periods of contact with the spacecraft per day. One period will coincide with normal daylight periods at Goddard and will last for approximately 8 hours. Near real time operations may take place at this time, with instrument commmands being uplinked almost immediately to the spacecraft. In practice, CDS will normally be operated automatically by the running of well developed operating command sequences stored in a time-tagged deferred command store on board. The two remaining, shorter spacecraft contact periods will be used for tape recorder dumps and the uplinking of large blocks of commands. In addition, there will be periods when 24 hour contacts are available.

Following the reception of telemetry data at the CDS EOF facility, a pipeline process will perform operations on the engineering and science telemetry data. Engineering data will be checked against an alarm limits database and calibrations applied for display in near real time on workstation display pages. The science data will be decompressed and automatically reformatted into FITS format files and stored locally, for later onward network transmission to the Experiment Analysis Facility (see below). All of the telemetry data is archived to disk for later retrieval. The CDS facility also has the capability to provide quick look analysis of the science data within the pipeline processing.

Telemetry data is also received from the SOHO tape recorder dumps as files via the Goddard SOHO facility. The same processing as applied to the near real time telemetry is applied to this replay data.

The near real time data and initial tape recorder data may contain data dropouts; 'final' spacecraft reprocessed data will also be received by CDS at the EOF some time after the near real time data. Again, these data will be processed in the same way, on arrival.

Science planning will take place at the EOF and the commands necessary for the real time operations and non-contact operations will be prepared utilising software on a master workstation at the CDS EOF facility. All commanding is accomplished via mnemonics, which are converted by software to blocks for uploading to the spacecraft. The software can be operated off-line to make syntax checks on the commanding. All mnemonics can be written into script files, which form logical operation units, and these are interpreted by the software.

Complementary to the CDS EOF operation is a CDS facility at the Experiment Analysis Facility (EAF). The CDS data, in FITS files, will be relayed to the EAF from the EOF. The FITS format ensures that the data are in a suitable state for easy inspection and analysis by the scientists at the EAF. CDS-dedicated workstations will be located at the EAF, for CDS and visiting staff to perform on-site analysis and interpretation. The analysis workstations have the capability of operating the EOF workstation software, as EOF 'clients', and can display either the near real time engineering or quick look science data. Thus, the EAF scientific staff may keep a close eye on the operations at any time. The main CDS data archive will also be based at the EAF and will include calibration data necessary for the correct interpretation of CDS data. Data from the facility will be passed to the main SOHO archive daily. CDS data can also be forwarded from the EAF to remote Co-Investigators as required. Full data distribution will be made weekly to the Principal Investigator institute and some Co-Investigator institutes on CD-ROM'S or Exabyte tape.

10. Scientific Operations

10.1. CDS Studies

The CDS experiment is extremely versatile. We may record spectra in any of the ranges defined above; we may raster the mirror and slit to produce images in any selected wavelengths; we may select appropriate spectral and spatial resolutions by selecting from a variety of slits; we have freedom to choose any reasonable accumulation times and fields of view, and we may point to any selected location on the Sun or in the low corona.

One limiting aspect of the operation of CDS is the telemetry rate. In normal operation we have a telemetry rate of 11.3 kbits/sec. If one notes that the spectra on the NIS detector take up approximately 1024 x 300 pixels, the counts from each of which may be recorded as a 12 bit word, it would take over 5 minutes to extract the data. This is for one spectrum,

which may be for a single location of a multipoint raster. This may be fine for some operations but is quite limiting for others, where time resolutions of seconds to minutes are needed. Thus we introduce on-board compression schemes and data selection - the observer is encouraged to select the portions of the spectra that he or she requires.

To cope with the flexibility of CDS, and the telemetry limitations, it is essential that a detailed consideration of operations relating to specific scientific studies be addressed. Since 1986, this has been done through annual CDS Science Team meetings and the CDS Science Report (Harrison, 1993), known as the CDS Blue Book.

Many scientific studies have been discussed and defined in some detail in the CDS Science Report. Indeed some 50 such studies now exist. These form the building blocks of the CDS scientific operation. They fall into three broad areas, namely, (i) synoptic sequences - for solar monitoring, (ii) calibration and monitoring sequences - to provide a continuous measure of the performance of CDS including cross-calibration with other SOHO instruments, and (iii) scientific sequences. Each study has been defined to the extent that the raster area, the slit, the dwell times, the lines selections, the compression schemes etc... have all been worked out. It is beyond the scope of this paper to reproduce all of this information for a selection of such schemes. However, below, we summarise the nature of five schemes to illustrate the approach. Each scheme is given a unique 5 letter ID which is given here.

1. Synoptic Study (SYNOP) - Daily full N-S Scan Along Central Meridian, NIS, 4 arcmin wide, using a 2 x 240 arcsec slit and collecting data for 16 prime lines. Used to construct EUV Carrington rotation maps to monitor global structure and evolution.

2. Spectral Atlas (SPECT) - GIS full spectrum returned for 15 x 15 locations (2 x 2 arcsec slit) over a 30 x 30 arcsecond field of view. Used to monitor the instrument through the regular measure of quiet Sun intensities and to provide a thorough analysis of the solar EUV spectrum.

3. High Velocity Event Study (HIVEL) - Rapid NIS raster over 30 x 30 arcseconds, using the 2 x 240 arcsecond slit. Line profiles from a range of lines of different temperatures of formation are monitored, to trace flows through the solar atmosphere. (With the resolving powers given above, we may expect to readily detect shifts of order several tens of km/s and greater).

4. Line Broadening with Altitude Study (BROAD) - GIS raster, using 2 x 2 arcsecond slit, over 2 x 200 arcsecond area extending well above limb. To identify line brodening due to wave activity as a function of altitude.

5. Mass Ejection Study (EJECT) - NIS scan of 4 x 4 arcmin area using 2 x 240 arcsecond slit, on potential mass ejection target (e.g. prominence), providing data from a range of emission lines giving diagnostic information on the target region.

Full details of the CDS studies already developed can be found in the Blue Book.

Some studies have been designed or refined in conjunction with other SOHO experiment teams to ensure that studies which require joint observations are accommodated. Several such schemes exist as so-called Joint Observing Programmes.

10.2. Operations Planning

There will be a regular commitment to synoptic and calibration/monitoring studies. For example, the synoptic study mentioned above will be done once per day, and GIS and NIS spectral atlases will be done frequently, to monitor the quiet Sun and invariant emission line intensity ratios, to assess the performance of CDS. The remaining observing time, which will comprise some 80% of the total, is devoted to science studies.

CDS long term planning meetings will discuss campaigns and strategies for the coming months. This will take the form of selecting groups of scientific studies to address specific scientific topics, for example, and the outcome of such selection will form the basis for the CDS input to SOHO-wide planning meetings. From the SOHO monthly planning meetings, we may schedule the study structure of up-coming weeks and refine them during daily planning sessions where, for example, the final target areas would be be selected.

These activities will be supported by consultations amongst selected members of the Co-Investigator team and by dedicated scientific staff at the EOF. Each study will be developed to "flight readiness" by using a CDS software science planning tool which, on completion, writes the appropriate command list. This would normally be tested on a test set-up involving the CDS engineering model prior to being uplinked to CDS.

10.3. Ground Software

The complexity of the CDS operation ensures that the ground software is necessarily complex. The CDS ground software package ensures that data are acquired correctly and stored, archived, distributed and logged as appropriate. It also provides planning tools for operations and study planning and construction, and quick look and detailed analysis routines. Most of the software is written in IDL and is tailored for use on Digital Alpha machines operating OSF.

Mouse driven plannning tools allow the scientist to select and view proposed sequences/operations and, if appropriate, to write the command lists to run them. In addition, planning tools exist to schedule CDS operations.

CDS data will be captured by the experiment workstation on arrival at the EOF and will be processed and stored. This will involve updating various catalogues which can be interrogated later by the scientist to identify data-

sets of interest. A full data-set archive will be available at the Goddard Space Flight Center, but also at the Principal Investigator institute.

The quick look analysis code allows a thorough first look at any data-set. Again, through mouse-driven interrogation, the user can examine any image or set of images and plot basic features such as line profiles, images and intensity-time curves, as well as make use of line identification schemes.

The detailed analysis routines extend this facility by including detailed scientific analysis codes such as the calculation and comparison of synthetic spectra, the calculation of differential emission measure (amount of material at different temperatures), the detailed analysis of intensity ratios to obtain diagnostic information. These include the provision of a well developed and properly assessed atomic data analysis procedure - the interpretation of solar information from spectral intensities is limited by our knowledge of the relevant atomic data. To this end, we have adopted and adapted the Atomic Data Analysis System (ADAS) which was developed at the Joint European Torus, Abingdon, UK (Summers, 1994).

11. The Consortium

The CDS experiment was developed and constructed by an international team led by the Rutherford Appleton Laboratory (RAL), UK. Hardware and software was supplied by groups at the Mullard Space Science Laboratory, UK (GIS detectors, EPS, CDHS hardware and software), the University of Oslo, Norway (electronic ground support equipment, ground software), the Goddard Space Flight Center, USA (VDS detectors, NI gratings, ground software), the Max Planck Instutute, Garching, Germany (telescope), the Physikalisch Technische Bundesanstalt, Berlin, Germany in conjunction with ETH, Zurich (calibration), University of California at Berkeley (VDS intensifier), as well as RAL (structure, spectrometer - including scan mirror, slit, mechanisms, MCU and harness, doors, pointing mechanism, ground and CDHS software, assembly, integration and test, contamination control, product assurance and overall management).

The Co-Investigator Science Team consists of: B. Aschenbach (Garching, Germany), A.M. Cruise (Chilton, UK), J.L. Culhane (Holmbury St Mary, UK), G. Doschek (Washington DC, USA), A.H. Gabriel (Orsay, France), M.C.E. Huber (Noordwijk, The Netherlands), C. Jordan (Oxford, UK), O. Kjeldseth-Moe (Oslo, Norway), M. Kühne (Berlin, Germany), J. Lang (Chilton, UK), H.E. Mason (Cambridge, UK), B. Monsignori-Fossi (Florance, Italy), K. Norman (Holmbury St Mary, UK), J.H. Parkinson (Holmbury St Mary, UK), B.E. Patchett (Chilton, UK), A.I. Poland (Greenbelt, USA), E.R. Priest (St Andrews, UK), J.H.M.M. Schmitt (Garching, Germany), O.H.W. Siegmund (Berkeley, USA), G.M. Simnett (Birmingham, UK), R.J. Thomas (Greenbelt, USA), W.T. Thompson (Greenbelt, USA),

J.G. Timothy (New Brunswick, Canada), G. Tondello (Padova, Italy) and J. Trümper (Garching, Germany). In addition, there is a group of 25 Associated Scientists. The CDS Project Manager is Eric Sawyer (RAL), the Principal Investigator is Richard Harrison (RAL) and the Project Scientist is Andrzej Fludra (RAL).

Acknowledgements

The CDS project has involved many individuals from engineers to solar physicists, from design staff to optics specialists, from managers to computer hardware and software people. The participating institutes and the science team have been listed above but here, we would like to thank individuals who have not already been noted who made a significant contribution to the CDS effort. At RAL, these include R.W.P.McWhirter, E.G. Capocci, F.S. Carr, C.A. Eley, P.E.G. Hingston, P.J. Horton, K.A. Lidiard, J.S. Long, J.A. Mackerness, N. Morris, L. Mullee, S.I. Harmer, A.R. Jackson, J. Pateman, P. Paynter, A. Pearce, G.E. Pullinger, P.D. Read, R. Roberts, M.R. Selley, T.B. Shaw, B.J. Smith, D. Stanley, J. Varley and K.L. Yeo. In addition, we would like to thank E. Alam, M.L. Edgar, R. Gowan, J. Lapington, P.H. Sheather, A. Smith and M. Trow at MSSL, N. Brynildson at the University of Oslo, M. Swartz and L.J. Payne at the Goddard Space Flight Center, W. Paustian and B. Wende at PTB, Berlin, G.W. Fraser at Leicester University and O. von der Lühe at the European Southern Observatory, Garching.

We would like to give special thanks to Bruce Patchett who, as the original CDS Principal Investigator (1986-1992) made CDS a reality.

References

Arnold, D. and Ulm, G.: 1994, 'Determination of photon emission probabilities of radionuclides', *Nucl. Instr. and Meth.* **339**. 43.

Barron, I.M.: 1978, 'The transputer', in (ed) Aspinall, D. 'The microprocessor and its application', Cambridge University Press, Cambridge, UK.

Bhatia, A.K. and Mason, H.E.: 1980, 'Theoretical atomic structure and electron scattering data for ions in the nitrogen isoelectronic sequence', *M.N.R.A.S.* **190**, 925.

Boucarut, R.A., Leviton, D.B., Thomas, R.J. and Madison, T.: 1993, 'Evaluation of the EUV toroidal diffraction gratings for SOHO/Coronal Diagnostic Spectrometer', *SPIE Proc.* **2011**, 565.

Breeveld, A.A., Edgar, M.L., Smith, A., Lappington, J.S. and Thomas, P.D.: 1992, 'A SPAN MCP detector for the Coronal Diagnostic Spectrometer', *Rev. Sci. Inst.* **63**, 1.

Dere, K.P., Mason, H.E., Widing, K.G. and Bhatia, A.K.: 1979, 'XUV electron density diagnostics for solar flares', *Ap.J. Suppl* **40**, 341.

Doyle, J.G., Mason, H.E. and Vernazza, J.E.: 1985, 'Interpretation of EUV spectra from loop structures in an active region at the limb', *Astron. Astrophys.* **150**, 69.

Dwivedi, B.N.: 1988, 'Electron density from Mg VIII emission lines', *Solar Phys.* **116**, 405.

Dwivedi, B.N. and Raju, P.K.: 1980, 'Density dependence of solar emission lines of boron-like ions', *Solar Phys.* **68**, 111.

Fischer, J., Kühne, M. and Wende, B.: 1986, 'Instrumentation for spectral radiant power measurements of sources in the wavelength range 5 to 150 nm', *Nucl. Instr. and Meth. A* **246**, 404.

Harrison, R.A.: 1993, 'The CDS Science Report - Blue Book', RAL publication SC-CDS-RAL-SN-93-0007, May 1993.

Harrison, R.A. and Sawyer, E.C.: 1992, 'The Coronal Diagnostic Spectromter for the Solar and Heliospheric Observatory', *Proc. 1st SOHO Workshop, ESA* **SP-348**, 17.

Harrison, R.A. and Sawyer, E.C.: 1993, 'The Coronal Diagnostic Spectrometer for the Solar and Heliospheric Observatory', *2nd SOHO Workshop, ESA SSD Publication* **S/93/386**, 21.

Harrison, R.A., Kent, B.J., Sawyer, E.C., Hollandt, J., Kühne, M., Paustian, W., Wende, B. and Huber, M.C.E.: 1995, Proc. NEWRAD conference, Berlin.

Heroux, L., Cohen, M. and Malinovsky, M.: 1972, 'The interpretation of XUV rocket measurement of intensity ratios of solar spectral lines in li-like ions', *Solar Phys.* **23**, 369.

Hollandt, J., Jans, W., Kühne, M., Lindenlauf, F. and Wende, B.: 1992, 'A beam line for radiant power measurements of VUV and UV sources in the wavelength range 40-400 nm', *Rev. Sci. Instrum.* **63**, 1278.

Hollandt, J., Huber, M.C.E. and Kühne, M.: 1993, 'Hollow cathode transfer standards for the radiometric calibration of VUV telescopes of the Solar and Heliospheric Observatory (SOHO)', *Metrologia* **30**, 381.

Hollandt, J., Kühne, M. and Wende, B.: 1994, 'High-current hollow-cathode source as a radiant intensity standard in the 40 - 125nm wavelength range', *Appl. Opt.* **33**, 68.

Janesick, J., Elliott, T. and Pool, F.: 1989, 'Radiation damage in scientific charge-coupled devices', *IEEE Trans on Nuclear Science*, **36**, 572.

Jordan, C.: 1965, 'The population of excited levels of the ground terms of ions Fe X, XI and XIV in the solar corona', *Phys. Lett.* **18**, 3, 259.

Jordan, C.: 1966, 'The abundance of iron in the solar corona', *M.N.R.A.S.* **132**, 515.

Keenan, F.P. and Aggarwal, K.M.: 1989, 'O III line ratios in the Sun', *Ap. J.* **344**, 522.

Keenan, F.P., Kingston, A.E., Aggarwal, K.M. and Widing, K.G.: 1986, 'Mg VII and Si IX line ratios in the Sun', *Solar Phys.* **103**, 225.

Keenan, F.P., Aggarwal, K.M. and Widing, K.G.: 1986, 'Theoretical Ne V emission line ratios compared to solar observations', *Solar Phys.* **105**, 47.

Kent, B.J., Swinyard, B.M. and Hicks, D.H.: 1993, 'Contamination effects on EUV optics in the space environment', *SPIE Proc.* **1945**, 348.

Kent, B.J., Swinyard, B.M. and Martin, E.L.: 1994, 'Contamination control and material screening for the extreme ultraviolet Coronal Diagnostic Spectrometer on SOHO', *SPIE Proc.* **2210**, 474.

Lang, J.: 1988, 'The measurement of NeV 2-2 line intensity ratios', *J. de Physique* **49**, C1-59.

Lidiard, K.A. and Gray, P.F.: 1991, 'The Optical Design of the Coronal Diagnostic Spectrometer (an Instrument for SOHO)', *Proc. Horizons de l'Optique et ICSO'91, CNES.*

Malinovsky, M.: 1975, 'New calculations of atomic data concerning EUV lines of O V', *Astron. Astrophys.* **43**, 101.

Malinovsky, M. and Heroux, L.: 1973, 'An analysis of the solar extreme ultraviolet spectrum between 50 and 300 Å', *Ap. J.* **181**, 1009.

Mason, H.E. and Bhatia, A.K.: 1978, 'Theoretical intensity ratios for the UV lines of Mg VII, Si IX and S XI', *M.N.R.A.S.* **184**, 423.

Mason, H.E. and Young, P.: 1994, *Proc. 3rd SOHO Workshop - ESA SP* In press.

Neupert, W.M., Epstein, G.L., Thomas, R.J. and Thompson, W.T.: 1992, 'An EUV imaging spectrograph for high resolution observations of the solar corona', *Solar Phys.* **137**, 87.

Patchett, B.E., Harrison, R.A., Sawyer, E.C. and co-authors: 1989, 'CDS - The Coronal Diagnostic Spectrometer for SOHO', *ESA SP-1104*, 39.

Riehle, F. and Wende, B.: 1985, 'Electron storage ring BESSY as a radiometric source of calculable spectral radiant power between 0.5 and 1000 nm', *Opt. Lett.* **10**, 365.

Schmidt, M., Dinger, U., Petasch, T. and Trebstein, F.: 1994, 'Wolter-Schwarzchild solar telescope. CDS flight model manufacturing and assembly Optical Technology for Space Instrumentation', *SPIE Proc* **2210**, 383.

Siegmund, O.H.W., Coburn, K. and Malina, R.F.: 1985, 'Investigation of large format microchannel plate Z configurations', *IEEE Trans on Nuclear Science* **32**, 443.

Summers, H.P.: 1994, 'Atomic Data and Analysis Structure: User manual', *JET Publication* **IR(94)06**.

Thompson, W.T., Poland, A.I., Sigmund, O.W., Swartz, M., Leviton, D.B. and Payne, L.J.: 1992, 'Measurements of an intensified CCD detector for the Solar and Heliosperic Observatory', *SPIE Proc.* **1743**, 464.

Vernazza, J.E. and Mason, H.E.: 1978, 'Density sensitivity of the solar EUV emission from Boron-like ions', *Ap. J.* **226**, 720.

Vernazza, J.E. and Reeves, E.M.: 1978, 'Extreme ultraviolet composite spectra of representative solar features', *Ap. J. Suppl.* **37**, 485.